

LA-UR-17-31501

Approved for public release; distribution is unlimited.

Title: Risk Assessment of Carbon Sequestration into A Naturally Fractured Reservoir at Kevin Dome, Montana

Author(s): Nguyen, Minh
Onishi, Tsubasa
Carey, James William
Will, Bob
Zaluski, Wade
Bowen, David
DeVault, Brian
Duguid, Andrew
Spangler, Lee
Stauffer, Philip H.

Intended for: Report

Issued: 2017-12-22

Disclaimer:

Los Alamos National Laboratory, an affirmative action/equal opportunity employer, is operated by the Los Alamos National Security, LLC for the National Nuclear Security Administration of the U.S. Department of Energy under contract DE-AC52-06NA25396. By approving this article, the publisher recognizes that the U.S. Government retains nonexclusive, royalty-free license to publish or reproduce the published form of this contribution, or to allow others to do so, for U.S. Government purposes. Los Alamos National Laboratory requests that the publisher identify this article as work performed under the auspices of the U.S. Department of Energy. Los Alamos National Laboratory strongly supports academic freedom and a researcher's right to publish; as an institution, however, the Laboratory does not endorse the viewpoint of a publication or guarantee its technical correctness.

LANL Deliverable to the Big Sky Carbon Sequestration Partnership

Risk Assessment of Carbon Sequestration into A Naturally Fractured Reservoir at Kevin Dome, Montana

Subtask R.3.7. Application of an Integrated Assessment Model (IAM) to the Kevin Dome site

December 31, 2017

Minh C. Nguyen, Tsubasa Onishi, , J. William Carey, Bob Will, Wade Zaluski, David H. Bowen, Bryan Devault, Andrew Duguid, Lee H. Spangler, Philip H. Stauffer

Executive Summary

In this report, we describe risk assessment work done using the National Risk Assessment Partnership (NRAP) applied to CO₂ storage at Kevin Dome, Montana. Geologic CO₂ sequestration in saline aquifers poses certain risks including CO₂/brine leakage through wells or non-sealing faults into groundwater or to the land surface. These risks are difficult to quantify due to data availability and uncertainty. One solution is to explore the consequences of these limitations by running large numbers of numerical simulations on the primary CO₂ injection reservoir, shallow reservoirs/aquifers, faults, and wells to assess leakage risks and uncertainties. However, a large number of full-physics simulations is usually too computationally expensive. The NRAP integrated assessment model (NRAP-IAM) uses reduced order models (ROMs) developed from full-physics simulations to address this issue. A powerful stochastic framework allows NRAP-IAM to explore complex interactions among many uncertain variables and evaluate the likely performance of potential sequestration sites.

Section 1 has an overview of the Big Sky Project with its original goals and current closeout objectives in the context of geological carbon storage as a climate change mitigation technology. To aid this effort, the NRAP toolset is utilized to carry out risk assessment calculations of a hypothetical CO₂ injection and the impact it may potentially have on surrounding receptors. A brief history of NRAP is also covered in this section.

Section 2 provides a summary of the characterization work at the Kevin Dome site to date and explains the significance of the acquired dataset. This work includes 3-dimensional seismic data, borehole and core measurements, and well test data that were acquired, processed, and interpreted during Phase II of the project. These data reveal critical insights into the structure of Kevin Dome, its potential storage formations, and the caprock layers that would safeguard the CO₂ plume in the event of actual injection.

Section 3 presents the risk assessment workflow used in this study. This section includes subsurface reservoir simulations generated from the Eclipse Compositional (E300) reservoir simulator that is considered an energy industry standard and is used as input to the NRAP toolset. Simulation results from E300 include reservoir pressure and CO₂ gas saturation distributions at each time-step of the injection and monitoring period. These time-dependent distributions were analyzed at the top layer of the CO₂ sequestration reservoir and used to create ROMs. The role of ROMs is to replace full-physics models and allow risk assessment calculations to be less computationally expensive. To calculate risk of CO₂ and brine potentially being leaked to an intermediate reservoir, underground sources of drinking water (USDW) aquifers, and the atmosphere, two models of wellbore and fault leakage pathways were employed.

Section 4 summarizes the risk assessment results and provides an analysis of uncertainty of a hypothetical CO₂ injection in the middle Duperow formation at the Kevin Dome site. This study demonstrates the usage of NRAP-IAM in assessing CO₂/brine leakage through both abandoned wells and fault pathways in a real field application. We identified key parameters for which potential CO₂ leakage is sensitive including fracture permeability, end-point CO₂ relative permeability, capillary pressure, and permeability of confining rocks. The number of NRAP Monte Carlo realizations necessary to reach a converged solution was about 500 to 600.

Table of Contents

Executive Summary	2
1. Introduction	6
2. Site Description	10
2.1. Reservoir Geology	11
2.2. Characterization Data	15
2.2.1. Seismic Data	15
2.2.2. Well Data	17
3. Methodology	18
3.1. Simulation Model	19
3.1.1. Model Description	19
3.1.2. Sensitivity Analysis	22
3.2. NRAP-IAM Model	28
3.2.1. Model Description	29
3.2.2. CO ₂ /Brine Leakage	34
3.2.3. Convergence	39
4. Results and Discussion	40
4.1. Sensitivity Analysis	40
4.2. Reservoir Simulation	42
4.3. NRAP-IAM Simulation	43
4.3.1. Wellbore Leakage	43
4.3.2. Fault Leakage	45
4.3.3. Convergence	48
4.4. Discussion	57
5. Summary and Future Work	58
6. References	59

Table of Figures

Figure 1-1: NRAP-IAM risk assessment workflow.....	8
Figure 2-1: Location map of the Kevin Dome Project showing the location of the project, sources of anthropogenic CO ₂ , and other large structural domes in the region.....	11
Figure 2-2: Tectonic map of Montana shows Kevin Dome As a large structural closure along the Sweetgrass Arch in north-central Montana. The inset window is an enlarged view of the surface geologic map of Kevin Dome.	12
Figure 2-3: a) Schematic east-west cross-section demonstrating trapping relationships of oil, natural gas, and CO ₂ on Kevin Dome. b) Stratigraphic column of geologic units at Kevin Dome.	13
Figure 2-4: Schematic cross-section showing the original technical approach that was envisioned for the project. Two principal wells were drilled to provide data for reservoir and site characterization, and to test production potential for CO ₂ from the Duperow Fm. (Danielson 33-17 well) and to test the potential injectivity (Wallewein 22-1 well).....	14
Figure 2-5: Fault interpretations by Schlumberger (after Zaluski, 2017).....	17
Figure 2-6: History matched Bottom hole pressure (after Onishi et al., 2017)	18
Figure 3-1: NRAP-IAM risk assessment workflow.....	19
Figure 3-2: Kevin Dome permeability model with the injector (Wallewein 22-1) in the middle of the domain.....	20
Figure 3-3: Sensitivity study workflow	23
Figure 3-4: Heterogeneous permeability fields (top layer of the injection zone). (a) Correlation length = 1000 (m), (b) Correlation length = 3000 (m), and (c) Correlation length = 5000 (m) ...	24
Figure 3-5: Relative permeability curves.....	25
Figure 3-6: Hysteresis relative permeability curves	25
Figure 3-7: Hysteresis of CO ₂ relative permeability in fracture (after Schlumberger, 2015).....	26
Figure 3-8: Capillary pressure curves in fracture and matrix	26
Figure 3-9: RROM-Gen extracted ROMs including elevation, fracture permeability, temperature, pressure, supercritical CO ₂ saturation, and dissolved CO ₂ weight fraction.....	28
Figure 3-10: Shallow permeable formations and legacy well locations. (a) shallow permeable formations (b) legacy well locations.....	29
Figure 3-11: The NRAP-IAM input panel for surface parameters.	29
Figure 3-12: The NRAP-IAM input panel for shallow aquifer statistical parameters.....	30
Figure 3-13: The NRAP-IAM input panel for defining legacy wells with known locations for well leakage calculation.....	31
Figure 3-14: NRAP-IAM input panel for fault swarm data.....	32
Figure 3-15: Illustration of geometrical construction of faults within a fault swarm ellipse. Major and minor axes of the swarm ellipse lie along the x and y axes, respectively. A) Faults are constructed using fault centroid, fault length, strike angle (θ), and pipe spacing parameter values. B) Multiple faults (and associated pipes) are constructed within the swarm ellipse. The evolving swarm is tested against the fault density parameter (faults per km) by way of a walk parallel to the ellipse minor axis; if the number of faults intersected exceeds the fault density, then the newest fault is discarded. Finally, the population of pipes in the swarm is truncated by the equation for the swarm ellipse.	33
Figure 3-16: Example fault swarms. Plus symbols denote the locations of individual pipes along the length of the fault. The faults have been truncated by the extent of the model domain.	34

Figure 3-17: ROM development flow diagram (from Harp et al. 2016)	36
Figure 3-18: Conceptual diagram of the geometrical elements of a fault, including host rock block, subvertical fault plane, fault core and damage zone, and discrete pipes for fluid flow along the fault plane.....	38
Figure 4-1: Sensitivity analysis results during injection period (4 years). (a) CO ₂ leakage to the atmosphere, (b) CO ₂ leakage to the intermediate aquifers, (c) CO ₂ leakage to the groundwater aquifer, (d) Brine leakage to the intermediate aquifers, (e) Brine leakage to the groundwater aquifer. The yellow bar represents the scenario when hysteresis is turned on.	41
Figure 4-2: Sensitivity analysis results during post-injection period (100 years). (a) CO ₂ leakage to the atmosphere, (b) CO ₂ leakage to the intermediate aquifers, (c) CO ₂ leakage to the groundwater aquifer, (d) Brine leakage to the intermediate aquifers, (e) Brine leakage to the groundwater aquifer. The yellow bar represents the scenario when hysteresis is turned on. See Table 3 for explanation of the parameters.	41
Figure 4-3: LHS results showing correlations among uncertain parameters	42
Figure 4-4: Reservoir simulation results including Total CO ₂ injection (MT) with P10, P50, and P90 as well as their respective fracture permeability (log(k)) distributions, fracture capillary pressure (P _{cf}), and matrix capillary pressure (P _{cm}).....	43
Figure 4-5: Impact of cement quality (shown as Very Bad to Very Good in the legend) on CO ₂ leakage to the atmosphere (left panel). The right panel presents parameters (fracture permeability, hysteresis curves, fracture capillary pressure, and matrix capillary pressure) in realizations that result in higher CO ₂ leakage.	44
Figure 4-6: CO ₂ /brine leakage (kg/s) into the atmosphere, intermediate reservoir, and groundwater aquifers versus time (year).....	45
Figure 4-7: Map view of CO ₂ plume resulting from leakage from a fault consisting of a series of leakage pipes with low and high fracture permeability cases at the end of 104 years.	46
Figure 4-8: CO ₂ plume and fault leakage of low and high fracture permeability case at the end of 104 years	47
Figure 4-9: CO ₂ leakage (kg/s) to an intermediate reservoir over time (year). The numbers on top of each graph represent the amount of NRAP-IAM Monte Carlo simulations performed.....	49
Figure 4-10: CO ₂ leakage (kg/s) to groundwater aquifers over time (year). The numbers on top of each graph represent the amount of NRAP-IAM Monte Carlo simulations performed.	51
Figure 4-11: CO ₂ leakage (kg/s) to the atmosphere over time (year). The numbers on top of each graph represent the amount of NRAP-IAM Monte Carlo simulations performed.	53
Figure 4-12: Brine leakage (kg/s) to intermediate reservoir over time (year). The numbers on top of each graph represent the amount of NRAP-IAM Monte Carlo simulations performed.....	54
Figure 4-13: Brine leakage (kg/s) to groundwater aquifers over time (year). The numbers on top of each graph represent the amount of NRAP-IAM Monte Carlo simulations performed.....	56
Figure 4-14: Error calculation results for NRAP-IAM.....	57

1. Introduction

Global warming is an environmental issue linked to the rise in global average temperatures because of increases in greenhouse gases such as carbon dioxide (CO₂) and methane in the atmosphere. Geologic carbon sequestration (GCS) has been proposed as a method to mitigate global warming (Metz et al., 2005). Candidate formations for GCS include depleted hydrocarbon reservoirs, unmineable coalbeds and saline aquifers (Bachu, 2000). Among them, saline aquifers are known to have the highest capacity for large scale subsurface storage (USDOE, 2015) and have been the formations of interest of multiple GCS projects around the world, including Australia (Stalker et al., 2014), Algeria (Ringrose et al., 2013), Norway (Singh et al. 2010), China (Nguyen and Stauffer, 2017), and the US (Soltanian et al., 2016). However, GCS in saline aquifers poses certain risks including CO₂ and brine leakage through abandoned wellbores or non-sealing faults into groundwater or to the earth surface. Large injection volumes of CO₂ could potentially induce seismicity through fault reactivation in the subsurface (Zoback and Gorelick, 2012; Bidgoli et al., 2014; Rinaldi et al., 2015). In addition to contributions to global warming, leakage of CO₂ and brine can threaten groundwater resources (Wilkin and DiGiuli, 2010; Keating et al., 2010; Trautz et al., 2012).

In an effort to better understand GCS, the US Department of Energy formed partnerships between industry, universities, and national laboratories to explore the viability of this concept in different regions of the United States. The Big Sky Carbon Sequestration Partnership's (BSCSP) Kevin Dome project is one of several Regional Carbon Sequestration Partnership Phase III Development projects with an intent to inject one million metric tons of CO₂ into a storage formation while validating site characterization, modeling and monitoring techniques. The target reservoir at Kevin Dome is the middle Duperow, a Devonian era carbonate (mixed dolostone and limestone) interval of ~100 ft thickness that produced CO₂ in drill stem tests of some historic wells near the apex of the dome but contains brine down dip. The original project scope planned to use the gas cap as the CO₂ source and the same reservoir in the down-dip brine leg as the storage target. This approach could provide some unique advantages: 1) wellbore data (logs and core) from the gas cap and brine leg would allow comparison of reactive reservoir rock and caprock exposed to CO₂ over geologic time vs. an engineered storage timescale providing insight on geochemical impacts on injection and storage; and 2) the concept of domes as storage hubs where CO₂ could be injected for storage and produced for enhanced oil recovery (thereby decoupling CO₂ production and utilization rates) could be tested.

In the process of the Kevin Dome site characterization, it was found that, counter to regional data trends, the targeted storage reservoir had less than 10,000 ppm total dissolved solids (TDS) which means it would be classified as an Underground Source of Drinking Water (USDW) by the primary criterion in the Environmental Protection Agency's (EPA) Underground Injection Control (UIC) regulations. The storage reservoir also had significant levels of H₂S and while most well classes allow for exceptions to the 10,000 ppm TDS minimum (e.g., if hydrocarbons or toxic substances are present at high enough levels), Class VI for CO₂ injection does not. Thus the project would be unable to secure a CO₂ injection permit. Nonetheless, valuable samples and data were acquired during the characterization including over 36 mi² of 3-dimensional, 9-component seismic data, and borehole data from two wells, one in the brine leg and one in the gas cap of a natural CO₂

reservoir including modern log suites and 45 ft of core of reactive reservoir rock and reactive caprock (the tight upper Duperow). The project has been re-scoped to utilize the existing samples and data to contribute to understanding CO₂ storage including the study reported here.

The scale of the BSCSP Kevin Dome project is typical of a GCS field site, and requires reservoir models spanning 10s-100s of km² in areal extent with a vertical extent of well over 1 km. In addition to a model for the injection reservoir, faults, existing wellbores, overlying USDWs, and leakage of CO₂ to the surface need to be considered. Coupled site models are used to make predictions about site behavior and to provide insight into site evolution. As data become available, models are refined to better simulate actual site behavior with a goal of reducing uncertainty and reducing risks to site operations. Risk proxies can be used to gauge possible impacts without calculating true risk values, a process that requires estimates of impacts that are often difficult to quantify. Risk proxies used previously include CO₂ injectivity; size of the Area of Review (AoR); CO₂ migration out of the injection horizon; and optimum location of monitoring wells (Dai et al., 2014).

One solution to creating a fully coupled system model is running high-fidelity, multiphase numerical simulations for an entire domain including a storage reservoir, shallow aquifers, wellbores, and faults across large spatial and temporal scales of GCS operation. Although this approach can address complex multiphase flow and trapping mechanisms, it requires fine spatial and temporal discretization to accurately model these complex physics that is usually computationally expensive. In addition, assessing these risks can easily require a large number of numerical simulations to span the many uncertainties and therefore this approach is not computationally attractive. Several (semi-)analytical models are available (Mathias et al., 2009; Nordbotten et al., 2005; Vilarrasa et al., 2013; Mijic et al., 2014; Zhou et al., 2017a; Zhou et al., 2017b). While analytical models provide significant benefits in terms of computational cost, these approaches cannot capture details such as permeability heterogeneity, which can be important in GCS.

Los Alamos National Laboratory initiated a hybrid (numerical plus analytical) system model, CO₂-PENS (Predicting Engineered Natural Systems: Stauffer et al. 2006; Pawar et al., 2006) which is an Integrated Assessment Model (IAM) used to determine CO₂ storage risk profiles. This tool was adapted to use as the base IAM for the US-DOE funded National Risk Assessment Partnership (NRAP) and the expanded tool, including contributions from several national laboratories (Carroll et al. 2016b), has been named NRAP-IAM (Pawar et al., 2016). NRAP-IAM simulates CO₂ storage reservoir security using reduced order models that are computationally efficient and allow analysis of the impact of uncertainty on prediction of leakage potential. NRAP-IAM decomposes the problem into interacting discrete components including a storage reservoir, wells, faults, intermediate reservoirs, shallow aquifers and the atmosphere. Each component has assigned properties with a range of uncertainties. For example, the pressure-saturation history of the CO₂ storage reservoir is represented using reduced order models (ROMs) developed from the results of full-physics simulations of CO₂ injection processes (Stauffer et al. 2015). Legacy wells within the area of interest have uncertainties in terms of total number, location, and wellbore integrity (Viswanathan et al. 2008, Hu et al., 2012; Jordan et al., 2015; Harp et al. 2016). Shallow drinking-water aquifers have uncertainties associated with permeability, porosity and thickness (**Figure 1-1**) (Keating et al., 2016; Carroll et al., 2016; Dai et al., 2014). NRAP-IAM allows the user to

explicitly define parameter values where data are available or to use generic properties obtained from the literature. The CO₂ storage system components are linked through potential CO₂ and brine pathways such as legacy wells and unsealed faults. Results of CO₂ migration are calculated in a Monte-Carlo framework in terms of 1) the amount of CO₂ present in the various model components, including reservoir and shallow formations, 2) the areal and volumetric extent of CO₂ plumes in the reservoir and shallow formations, and 3) components potentially impacted by CO₂ migration, such as shallow groundwater wells. The powerful stochastic framework allows NRAP-IAM to explore complex interactions among a large number of uncertain variables and to help evaluate the likely performance of potential sequestration sites.

Based on an algorithm developed at LANL, King (2016) built the Reservoir Reduced Order Model–Generator (RROM-Gen), which is a tool to convert reservoir simulation outputs from full-physics codes into lookup tables necessary to run the NRAP-IAM for uncertainties in a storage reservoir. RROM-Gen can utilize reservoir simulation data from a number of different simulators such as FEHM (Zyvoloski, 2007), TOUGH2 (Pruess et al., 1999), STOMP (White et al., 2012), ECLIPSE (Schlumberger), and GEM (CMG). RROM-Gen extracts CO₂ saturations and dissolved concentrations, temperature, and pressure from the top layer¹ of the injection reservoir to use as input for risk analysis in NRAP-IAM. Bilinear interpolation is performed to map full-physics calculations and input data on reservoir properties including elevation, permeability, temperature, pressure and CO₂ saturations and dissolved concentrations onto the 100x100 grid used within the NRAP-IAM. Note that the conversion is performed for every time step for dynamic data. The interpolated sets of properties, RROMs, provides a distribution of values for the uncertain parameters characterizing performance of the storage reservoir (**Figure 1-1**).

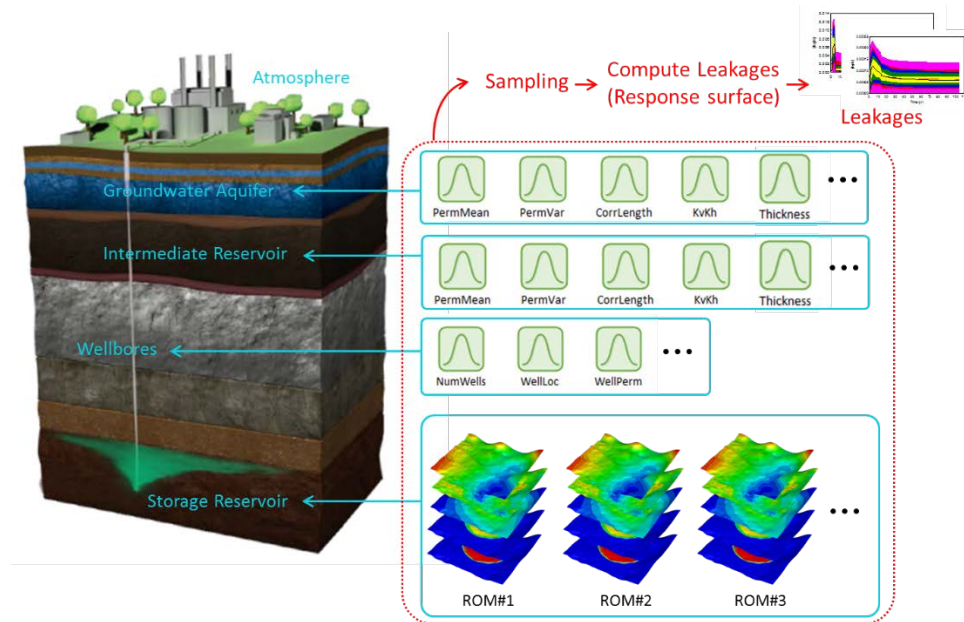


Figure 1-1: NRAP-IAM risk assessment workflow

¹ Only the top layer is used as representing the source term for leakage into wells and faults.

Viswanathan et al. (2008) and Stauffer et al. (2009) applied CO₂-PENS to CO₂ sequestration scenarios in synthetic cases including a depleted oil reservoir and saline aquifers. In these studies, CO₂-PENS had multiple options for leakage through wellbores including analytical wellbore leakage modules created by the Princeton-CMI group (Nordbotten et al., 2008) and the use of a multiphase-numerical simulator Finite Element Heat and Mass-Transfer (FEHM) (Zyvoloski, 2007). The first option was validated with CO₂ sequestration scenarios in simple homogeneous cases for a 2500 day period by comparing with numerical simulation results using ECLIPSE (Nordbotten et al., 2008). The comparisons show deviations in early time because of numerical dispersion in ECLIPSE and good agreement at late time. However, there is no guarantee that the analytical solution can maintain accuracy after the short period (2500 days) because assumptions in the analytical solution may not be valid over tens to hundreds of years, which is a typical CO₂ storage and monitoring scenario. While analytical models may be applicable to simple scenarios, they may not be capable of field case studies involving complexities such as heterogeneous permeability distributions. Although accurate, the second option to use FEHM to model wells can be computationally expensive if uncertainties are high and a large number of simulations is needed. To overcome this, Jordan et al. (2015) and Harp et al. (2016) developed wellbore leakage ROMs using response surfaces based on thousands of multiphase numerical simulations (using FEHM). The Multivariate Adaptive Regression Splines (MARS) algorithm (Frieman, 1991) was used to extract wellbore leakage ROMs that capture trends of leakage rates by numerical simulations. In the ROM approach, assumptions required in analytical solutions are not required and the computational burden is no longer a concern. Jordan et al. (2015) implemented the wellbore leakage ROMs into CO₂-PENS and used underlying reservoir simulations from the Kimberlina site in central California with several simplifications (Birkholzer et al., 2011b). A hypothetical set of five legacy wells were used in the application. Wellbore permeabilities were sampled from a random distribution and 54 full reservoir simulations of CO₂ injection into the Kimberlina reservoir were conducted, and the reservoir simulation results were converted into lookup tables and sampled using uncertain parameters in the storage reservoir.

Although hypothetical, this application showed the utility of the wellbore ROM in being able to quantify the CO₂ and brine leakage risks quickly. However, the sampling method in NRAP-IAM still remains a challenge: the number of numerical simulations required in this approach increases exponentially corresponding to the number of uncertain parameters. Specifically, the logic used in the Kimberlina example requires a minimum of $3N$ simulations, where N is the number of uncertain parameters and the multiplier '3' corresponds to low, base and high values spanning the range of each parameter in a simple box design. There are three uncertain parameters including permeability, pore compressibility, and porosity in the Kimberlina example, with 6 levels given to the most sensitive reservoir permeability (Birkholzer et al., 2011). Thus the number of reservoir simulations required is $6 \times 3 \times 3 = 54$. Although this approach is faster than running numerical simulations for an entire domain including a storage reservoir, shallow formations and legacy wells, it can be computationally prohibitive in field case applications because there are usually more than three significant uncertainties (Yoshida, 2016) such as relative permeability and capillary pressure and a single simulation can take days. A number of simulation studies and uncertainty quantifications of GCS have been done (Eigestad et al., 2009; Bao et al., 2013; Barrufet et al., 2010; Birkholzer et al., 2011; Pawar et al., 2014; Jordan et al., 2015; Dai et al., 2014; Harp et al., 2016; Nguyen et al., 2017a; Nguyen et al., 2017b). However, these only focus on a storage reservoir or include wellbore leakages but with a limited number of uncertain parameters.

Consequently, in this report we develop a new workflow in which we employ the Latin Hypercube Sampling (LHS) parameter sampling method to generate realizations of numerical simulations for the storage reservoir. LHS is a stratified-random procedure and provides an efficient way of sampling parameters from their distributions (McKay et al., 1979; Iman and Conover, 1980). Unlike random sampling, LHS ensures a full coverage of the range of each parameter by maximally stratifying each marginal distribution. Fewer numerical simulations are required to cover the same range of uncertainties in the developed workflow compared to previous approaches. Alternatively, with the same number of numerical simulations, the LHS approach can investigate more parameters. The new workflow allows NRAP-IAM to perform risk assessment for field scale applications using fewer underlying reservoir simulations resulting in lower computational burden.

To demonstrate the new workflow, this report presents the first application of the newly released, online, NRAP toolset to a Phase III Regional Carbon Sequestration Partnership dataset. We apply NRAP-tools to a fractured saline storage reservoir located at Kevin Dome in Montana. Data included in the analysis include a 3-D seismic survey, examination of existing boreholes in the region that penetrate the proposed Big Sky injection horizon, hydraulic testing on the proposed injection well, core analysis and permeability testing, site topology, and groundwater chemistry. Using the Schlumberger reservoir simulator, Eclipse, we generate simulations of CO₂ injection to explore uncertainty analysis within the NRAP-IAM tool. We investigate a variety of uncertain reservoir parameters including permeability, porosity, relative permeability, hysteresis of relative permeability, capillary pressure, fracture density, and salinity of the aquifer. Sensitivity of the NRAP-IAM model results to leakage of both brine and CO₂ are used as criterion to down-select to six primary uncertain variables. These six variables are then used to generate a set of 50 LHS reservoir simulations, reducing the number of simulations needed from 300 as reported by Dai et al. (2014). The reservoir simulations are extracted to lookup tables and used as input to the NRAP-IAM where leakage uncertainty distributions are generated. We also present estimates of the mass of CO₂ that could be injected during a four-year period at this site and compare results from the new method with a simpler method used previously. Finally, convergence of the results with increasing numbers of NRAP-IAM simulations is discussed.

2. Site Description

The Big Sky Carbon Sequestration Partnership (BSCSP) has investigated Kevin Dome, located in Toole County, north-central Montana (**Figure 2-1**), and its naturally occurring CO₂ as an analog for carbon storage and as a potential site for additional storage of anthropogenic CO₂. Detailed site characterization, laboratory core studies, well tests, and geologic/geophysical models coupled with operational data have deepened our understanding of the use of site characterization data for predicting geologic system performance. Additionally, this work has improved our understanding of the largest naturally occurring trap of CO₂ in the northwestern United States.

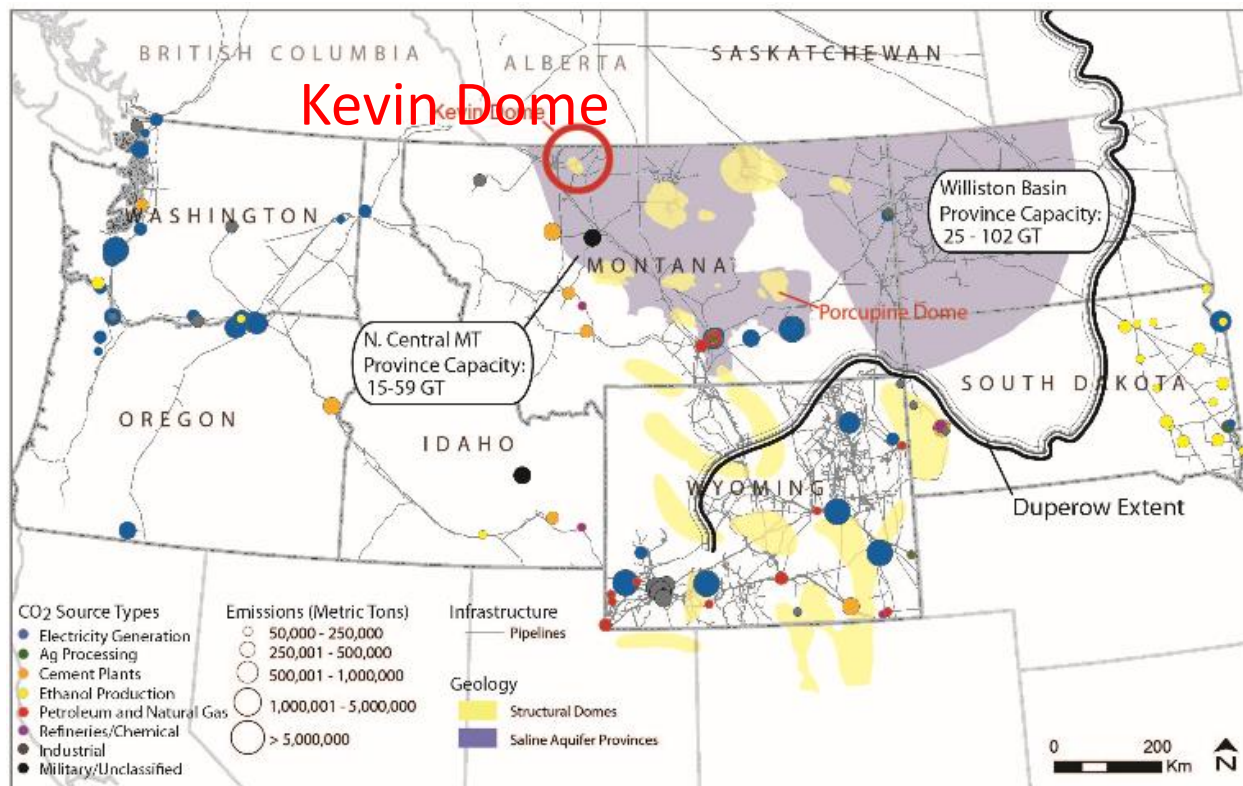


Figure 2-1: Location map of the Kevin Dome Project showing the location of the project, sources of anthropogenic CO₂, and other large structural domes in the region.

2.1. Reservoir Geology

Kevin Dome is a large structural dome formed as a culmination along the Sweetgrass Arch (**Figure 2-2**). The dome covers approximately 700 square miles (1800 square kilometers) at the Devonian Duperow stratigraphic level with approximately 750 feet (229 meters) of structural relief. Naturally occurring CO₂ has been documented from several oil and gas wells that have tested the Duperow formation over the past 50 years, but the volume, continuity of the trapped gas, and circumstances of its entrapment have been poorly understood. This dome is integral to trapping oil, natural gas and CO₂ (**Figure 2-3**) and has produced oil and natural gas since its discovery in 1922. Naturally occurring CO₂ is trapped in two major dolomite porosity zones within the Devonian Duperow formation. Oil and natural gas are trapped in a shallower limestone and sandstone reservoirs (**Figure 2-3**).



Figure 2-2: Tectonic map of Montana shows Kevin Dome As a large structural closure along the Sweetgrass Arch in north-central Montana. The inset window is an enlarged view of the surface geologic map of Kevin Dome.

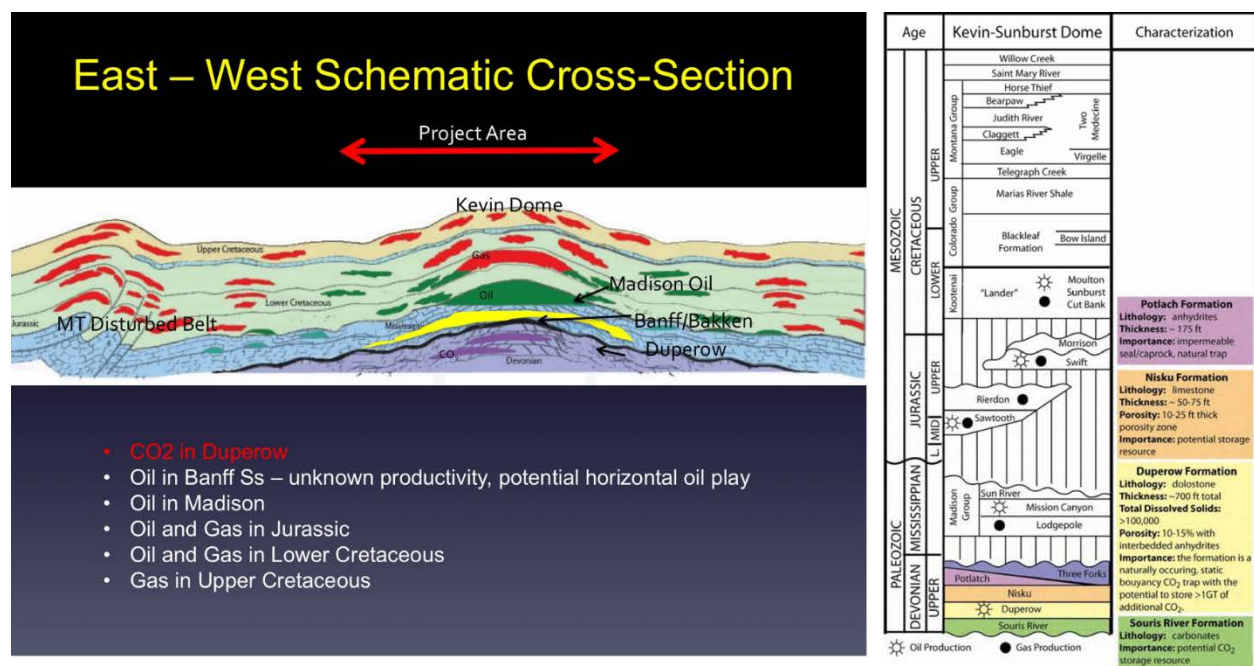


Figure 2-3: a) Schematic east-west cross-section demonstrating trapping relationships of oil, natural gas, and CO₂ on Kevin Dome. b) Stratigraphic column of geologic units at Kevin Dome.

The primary objective of the Big Sky Carbon Sequestration Partnership Phase III project was to extract up to 1 million metric tons of CO₂ from the naturally occurring CO₂ reservoir in the Duperow formation and re-inject it into the brine-filled portion of the Duperow formation at the flank of Kevin Dome (**Figure 2-4**). This project was to demonstrate that the target formation and other analogous formations are viable and safe targets for sequestration of a large fraction of the region's CO₂ emissions. The success criteria for the project would have been to safely inject CO₂ into the storage formation and through models and monitoring indicate permanence of storage in the reservoir. The research objectives were to improve the understanding of injectivity, capacity, and storativity in a regionally significant formation.

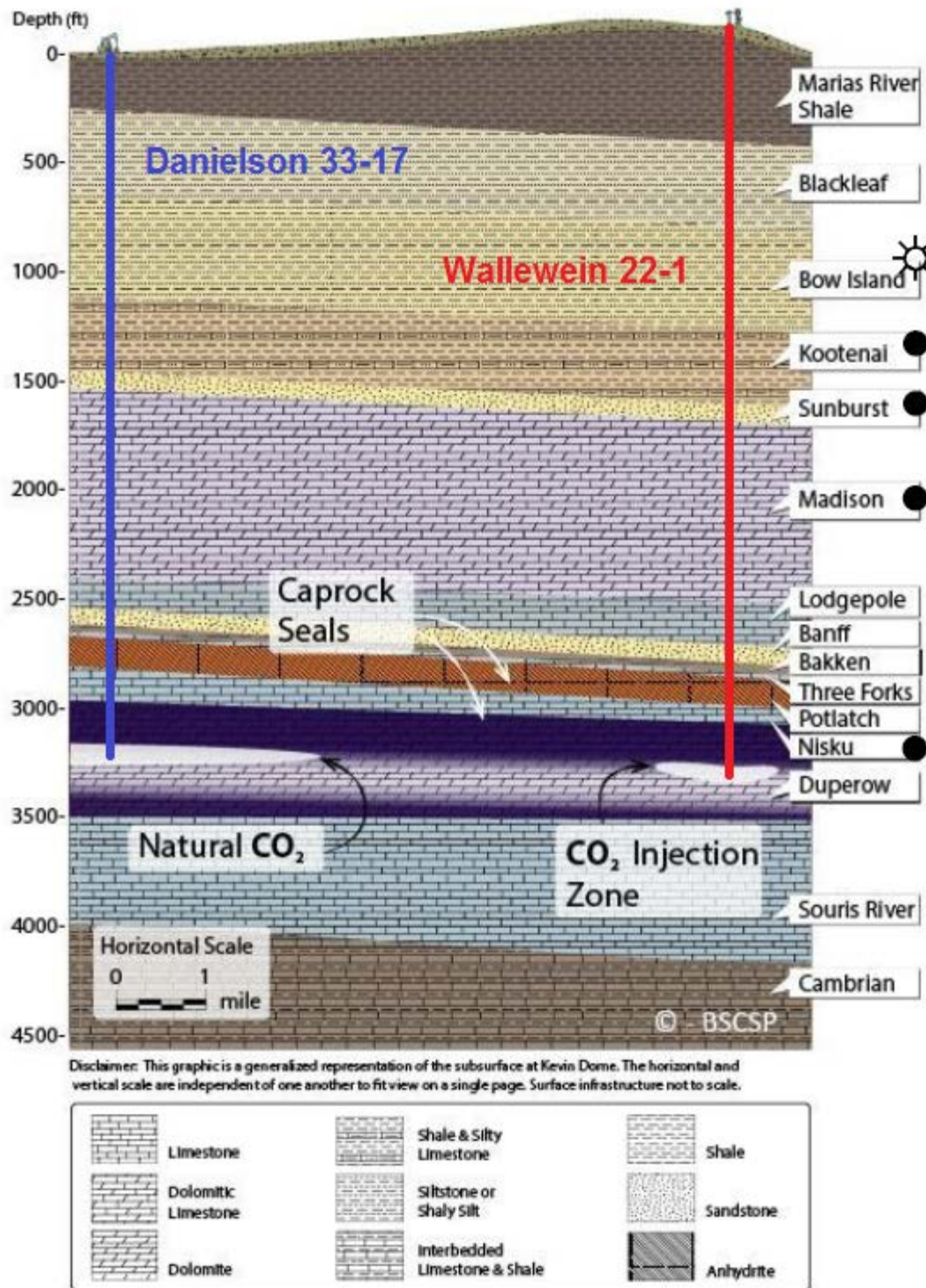


Figure 2-4: Schematic cross-section showing the original technical approach that was envisioned for the project. Two principal wells were drilled to provide data for reservoir and site characterization, and to test production potential for CO₂ from the Duperow Fm. (Danielson 33-17 well) and to test the potential injectivity (Wallewein 22-1 well).

After extensive efforts by BSCSP, the objective to extract up to 1 million metric tons of CO₂ from the naturally occurring CO₂ reservoir in the Duperow formation and re-inject it into the brine-filled portion of the Duperow formation proved to be unachievable for two reasons: (1) although the natural CO₂ was present as expected, BSCSP was unable to produce the CO₂ in large quantities due to phase transitions of the CO₂ in the reservoir; and (b) the total dissolved solids (TDS) of the brine in the targeted injection formation (Duperow) is less than 10,000 parts per million, which is lower than the TDS allowed (no exceptions) for carbon storage under U.S. EPA UIC Class VI injection rules. Neither of these outcomes were predicted from pre-characterization data. Given that the original objective of the BSCSP Phase III project cannot be achieved, the primary objective of the project has been revised to maximize the value of the existing data to DOE's Carbon Storage Program.

2.2. Characterization Data

2.2.1. Seismic Data

Given the anticipated presence and importance of natural fracturing in the targeted Duperow formation, the partnership acquired a multicomponent 3D seismic survey to characterize faulting, natural fractures and porosity heterogeneity in the Duperow. The 9 component 3-dimensional (9C-3D) seismic survey was acquired over three winter field seasons using both shear-wave vibrators and conventional P-wave vibrators. The chosen survey design was a relatively dense, symmetrically-sampled orthogonal layout with equal shot and receiver intervals of 110 feet. The corresponding shot and receiver line intervals were 880 and 660 feet respectively. The rectangular recording spread comprised 12 receiver lines, each having 96 channels, which delivered a very good azimuth and offset distribution for inversion of the data for both azimuthal anisotropy parameters and quantities reliant on high-quality long offset information from the horizontal and vertical shear wave (SH and SV) datasets such as density. Each receiver group consisted of a single digital three-component MEMS sensor augured into the ground with dedicated hand drills.

The first phase of the survey comprised the acquisition of approximately 8.5 square miles of 9C-3D data from January to March 2012. The second phase, acquired in the Winter of 2012/2013, resulted in the addition of 19 square miles of data and the final field season in the Winter of 2013/2014 completed data acquisition, resulting in a final survey area of approximately 36 square miles. Notable challenges during acquisition included both extremely cold and warm weather and the ensuing freeze/thaw cycles that greatly slowed field operations, as well as an unexpectedly large number of archeological sites which had to be delineated and avoided by the seismic acquisition crew.

Data processing for each mode included the traditional steps of geometry assignment and trace edits; compression (P) and shear (S) wave refraction statics using a general linear inversion (GLI) technique; eigenimage ground roll attenuation followed by conventional residual statics and velocity analysis; final noise attenuation in the cross-spread domain; and prestack time migration. Additional steps specific to the multicomponent data included source and receiver rotation (only receiver rotation in the case of the P, S data) and polarization analysis to determine the appropriate anisotropic symmetry system for further processing. Apart from a small area in the northeastern portion of the survey, no measurable azimuthal anisotropy was observed on the shear data, so

further processing for the SH, SV, and PS data was performed in a radial-transverse frame after layer stripping the shallow anisotropy observed in the area that did possess azimuthal anisotropy. The PS dataset also required common conversion-point binning due to the asymmetric raypaths characteristic of this mode.

After processing, each individual mode was interpreted for structure and amplitude variations corresponding to changes in rock properties in the overburden and target section. An essential part of the interpretation included a joint inversion of the P data with all of the multicomponent data to generate bandlimited P and S impedance and density volumes on the P time scale. These datasets were depth converted with depth structure maps created by integrating well tops with their corresponding seismic events at the Bow Island, Sunburst, Potlach, mid-Duperow porosity zone, and Souris River horizons and the resulting 3D seismic volumes were used to constrain the reservoir model built for the project.

Figure 2-5 depicts the seismic data area (map view) and interpreted faults by Schlumberger (marked as black) using edge detection. Though there are potentially about 11 faults in the study area, only one closest to Wallewein 22-1 to the West is considered in this modeling study as it is more likely to pose a possibility of leakage. The fault is incorporated into NRAP-IAM as a leakage pathway, along with legacy wells, to calculate the potential CO₂ and brine leakage rates to an intermediate reservoir and shallow groundwater aquifers.

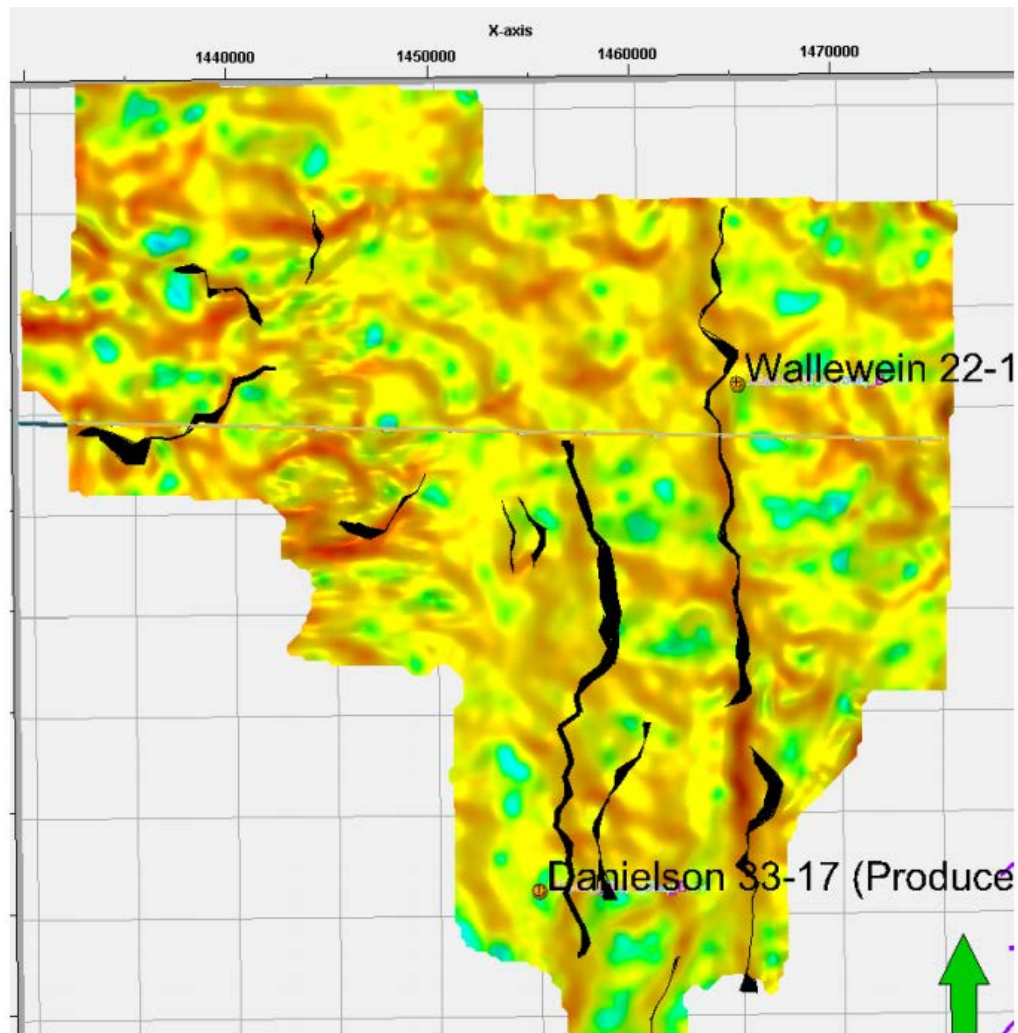


Figure 2-5: Fault interpretations by Schlumberger (after Zaluski, 2017)

2.2.2. Well Data

Two wells, the Danielson 33-17 (the first of several proposed production wells to supply CO₂ for the project) and the Wallewein 22-1 (a characterization and monitoring well near the proposed injection site) were drilled to depths below the base of the Duperow formation. The wells were cored in the major Duperow reservoir porosity zone and in primary and secondary caprock seals, and were logged with a detailed suite of tools including gamma ray, neutron porosity, total porosity, effective porosity, neutron magnetic resonance, and other physical variables. An extensive well testing program was implemented in both wells to test reservoir and fluid properties. It was discovered that CO₂ could not feasibly be produced from Danielson 33-17 and the salinity was too low in the middle Duperow formation to be able to obtain a Class VI UIC permit from EPA.

A step-rate injection and pressure fall-off test was conducted by Northern Lights Energy Company and Sanjel on the Wallewein 22-1 well in Toole County, Montana, from March 18, 2015, to March 27, 2015. Tandem electronic quartz gauges were run into the well on March 18, taking gradient

stops every 300 feet going into the well. Gauges were set at 4019 ft, and injection of 3% NaCl water began on March 19, 2015, at 09:57 a.m. After completion of all testing, gradient stops were also taken every 300 ft while coming out of the well. Due to operational difficulties with the flowmeter, the injection rates for days 2 and 3 were initially reported to be -854 barrels of water injected per day (bwipd) on day 2, and a final rate of -2000 bwipd on day 3. It was subsequently determined that day 2 and 3 rates were incorrect, thus, it was believed that determining the average injection rate based on volumes pumped would be most accurate. Therefore, for day 2 of injection, an average injection rate of 664 bwipd was used for a pumped volume of 225 barrels (bbls), and for day 3, an average injection rate of 686 bwipd was used for a pumped volume of 248 bbls. After injection, the final fall-off period was extended to 135 hours.

Bottom-hole pressure data were matched by Onishi et al. (2017) by modifying permeability values in the vicinity of Wallewein 22-1 (**Figure 2-6**). A different initialization was implemented to achieve matrix and fracture permeability calibration that is more aligned with that reported by Zhou et al. (2013). Calibrated permeability was then used to populate reservoir properties in the later part of our study.

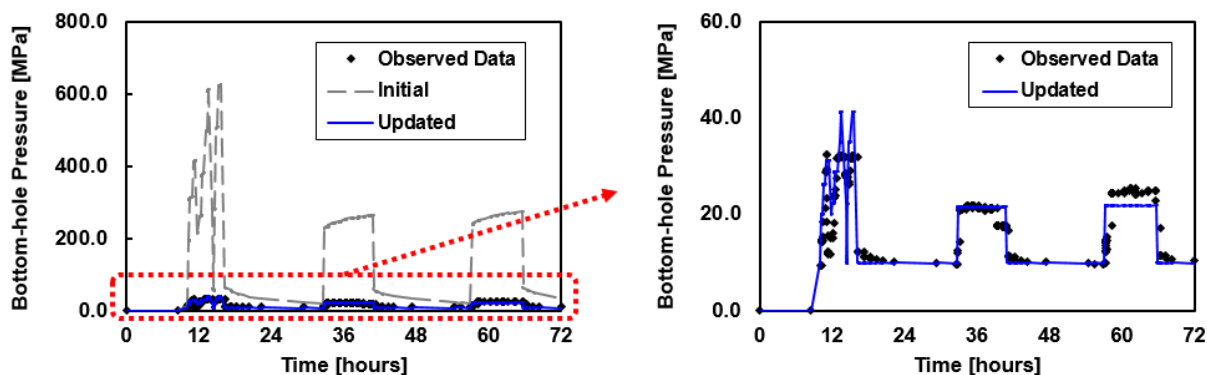


Figure 2-6: History matched Bottom hole pressure (after Onishi et al., 2017)

3. Methodology

This section presents the risk assessment workflow (**Figure 3-1**) with the following three primary elements: 1) model parameterization and sensitivity analysis, 2) reservoir simulation, and 3) CO₂/brine leakage computations.

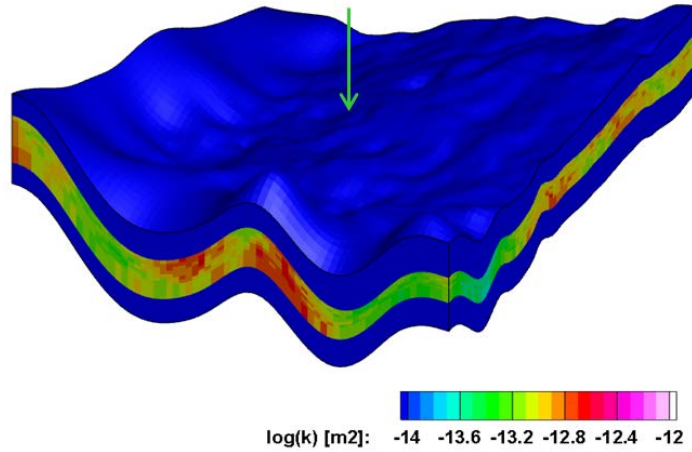


Figure 3-2: Kevin Dome permeability model with the injector (Wallewein 22-1) in the middle of the domain.

The geologic model includes a low permeability caprock and basement as part of the CO₂ storage system. The caprock and the basement were upscaled into single layers with average thickness of 60 m. Geological data described above show the existence of fractures with a relatively low permeability contrast between fracture and matrix (Spangler, 2016). A dual porosity-dual permeability model (Warren and Root 1963; Blaskovich et al., 1983) was therefore adopted to model fractures because matrix-matrix connections are important, and yet knowledge of fracture distributions is too limited for use of discrete fracture models (Noorishad and Mehran, 1982; Monteagudo and Firoozabadi, 2004; Hyman et al., 2015) nor the embedded discrete fracture model (Li and Lee, 2006; Moinfar, 2013).

The fluids modeled in this study using the CO2STORE (Schlumberger, 2015) facility in E300 for CO₂ storage in the saline aquifer are described by aqueous, gaseous and solid phases, with three components: water (H₂O), carbon dioxide (CO₂), and salt (NaCl) respectively. It is assumed to be an isothermal system (Pruess and Garcia, 2002). Mutual solubilities of CO₂ and H₂O are calculated to match experimental data for typical CO₂ storage conditions as described in by Spycher and Pruess (2005), based on fugacity equilibrium between water and a CO₂ phase. Aqueous fugacity was obtained by Henry's law, while CO₂ fugacity was calculated using a modified Redlich-Kwong equation of state (EOS; Redlich and Kwong, 1949). The gaseous density was obtained by the modified Redlich-Kwong equation of state, where the attraction parameter is temperature dependent (Spycher and Pruess, 2009). The CO₂ gaseous viscosity was computed based on results from Vesovic et al. (1990) and Fenghour et al. (1998).

In our approach, the Corey equations (Corey, 1954) were applied for relative permeability curves.

$$k_{r,CO_2} = k_{r,CO_2}^0 \left(\frac{S_{CO_2} - S_{CO_2,ir}}{1.0 - S_{CO_2,ir} - S_{brine,ir}} \right)^m \quad (1)$$

And

$$k_{r,brine} = k_{r,brine}^0 \left(\frac{S_{brine} - S_{brine,ir}}{1.0 - S_{CO_2,ir} - S_{brine,ir}} \right)^n \quad (2)$$

where, $k_{r,l}^0$ is the end-point relative permeability of phase l , S_l is the saturation of phase l , $S_{l,ir}$ is the irreducible saturation of phase l , and m and n are the curvature exponents of CO_2 and brine, respectively. The straight-line relative permeability curves are commonly used in dual continuum models (Romm, 1966) for fracture relative permeability. However, it is experimentally and numerically proven that the straight-line relative permeability curves are not always valid (Fourar et al., 1993; Pieters and Graves, 1994). Therefore, we follow previous simulation studies at this site (Zhou et al., 2013), in which non-idealized relative permeability curves are used for fracture relative permeability. **Table 1** provides a summary of parameters used in Equation (1) and Equation (2) following Pruess and Garcia (2002) and Zhou et al. (2013).

TABLE 1: Parameters for relative permeability model (from Zhou et al. 2013)

Parameter	Values
Fracture	
End-point CO_2 relative permeability, k_{r,CO_2}^0 (-)	0.50
End-point brine relative permeability, $k_{r,brine}^0$ (-)	0.15
Irreducible CO_2 saturation, $S_{CO_2,ir}$ (-)	0.10
Irreducible brine saturation, $S_{brine,ir}$ (-)	0.30
Exponent for CO_2 relative permeability, m (-)	2.0
Exponent for CO_2 relative permeability, n (-)	5.0
Matrix	
End-point CO_2 relative permeability, k_{r,CO_2}^0 (-)	0.30
End-point brine relative permeability, $k_{r,brine}^0$ (-)	0.05
Irreducible CO_2 saturation, $S_{CO_2,ir}$ (-)	0.25
Irreducible brine saturation, $S_{brine,ir}$ (-)	0.30
Exponent for CO_2 relative permeability, m (-)	2.0
Exponent for CO_2 relative permeability, n (-)	5.0

The capillary pressure model used in this work is the Van Genuchten (1980) model:

$$P_c = P_0 \left(\left(S^* \right)^{\frac{1}{\lambda}} - 1.0 \right)^{1.0-\lambda} \quad (3)$$

where, P_0 is the strength coefficient, λ is the pore size distribution index, and the normalized brine saturation S^* is given by

$$S^* = \frac{S_{brine} - S_{brine,ir}}{1.0 - S_{brine,ir}} \quad (4)$$

Table 2 presents parameter values in Equations (1) through (4) for the base case following (Pruess and Garcia 2002; Zhou et al., 2013). Note that the same capillary pressure curves are used in the fracture and matrix domain.

TABLE 2: Parameters for capillary pressure model (from Zhou et al. 2013)

Parameter	Values
Strength coefficient, P_0 (bar)	0.30
Exponent, λ (-)	0.457
Irreducible brine saturation, $S_{brine,ir}$ (-)	0.30
Maximum capillary pressure (bar)	5.0

The model consists of a single injection well located in the center of the storage formation. The well, assumed to be connected to all layers in the injection zone, has a wellbore radius of 0.07 m (Zhou et al., 2013) and injects supercritical CO₂ with a constant temperature of 34.4 °C and bottom-hole pressure (BHP) control of 18.5 MPa which is based on the hydro-fracture limit for the Duperow formation (Dai et al., 2014). We applied a pore volume multiplier of 3000 in boundary cells to mimic a continuous aquifer which is essentially equivalent to a constant pressure boundary (Juanes et al., 2006) while no-flow boundary conditions were applied to lateral boundaries as defaulted in E300. Initial temperature and pressure were set at 34.4 °C and 10.0 MPa at the top of the injection zone, which is based on the geothermal gradient and hydrostatic pressure gradient (Zhou et al., 2013). The initial condition implies that injected CO₂ will be in a supercritical state in the reservoir. The CO₂ injection period lasts for 4 years and the CO₂ plume is monitored over a period of 100 years post-injection which is a sufficient duration for the system to be at equilibrium. Because the CO₂ injection was simulated at constant pressure for a fixed period of time, the total amount of CO₂ injected was varied depending on the reservoir parameter obtained from the LHS.

3.1.2. Sensitivity Analysis

The first step is to identify the key performance parameters that characterize CO₂ and brine leakage. Workflow of this sensitivity analysis follows Hill (2010) and Olalotiti-Lawal et al. (2017) and is presented in **Figure 3-3**. The list of parameters included in the sensitivity analysis is provided in **Table 3**. The table also contains the range of values of each of the parameter used.

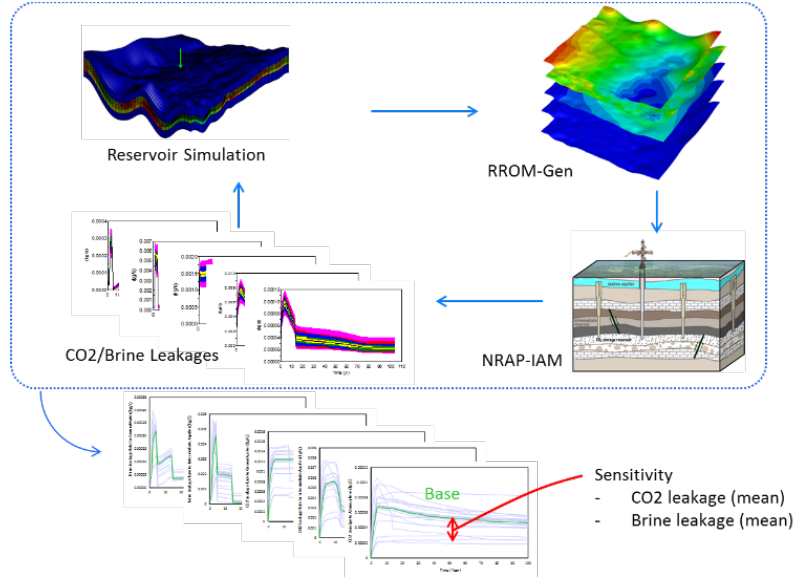


Figure 3-3: Sensitivity study workflow

TABLE 3: Reservoir, caprock and basement parameters and the range of assigned values

Parameter	Description	Low	Base	High
kf	Fracture mean permeability (m ²)	3.9e-14	5.9e-14	7.8e-14
kf_Corr	Correlation length for fracture permeability, (m)	1000.0	3000.0	5000.0
kvkh	Vertical fracture permeability anisotropy (-)	0.02	0.50	1.0
k_confrock	Permeability of caprock and basement (m ²)	3.0e-4	3.0e-2	3.0
km	Matrix permeability (uniform), (m ²)	1.0e-14	2.0e-14	3.0e-14
krfCO ₂ _end	End point CO ₂ relative permeability in fracture, (-)	0.30	0.50	0.70
krmCO ₂ _end	End point CO ₂ relative permeability in matrix, (-)	0.10	0.30	0.50
krfCO ₂ _Hyst	Hysteresis of CO ₂ relative permeability in fracture, (-)	ON and OFF		
P0f	Strength coefficient of fracture capillary pressure (bar)	0.20	0.30	0.40
P0m	Strength coefficient of matrix capillary pressure (bar)	0.20	0.30	0.40
sigma	Shape factor (m ⁻²)	0.12	1.2	5.0
Salinity	Salinity of the aquifer (ppm)	1.0e+4	2.0e+4	3.0e+4

The values and ranges of fracture and matrix permeability related parameters are based on previous simulation studies at this site (Dai et al., 2014; Zhou et al., 2013). We used constant values for matrix permeability and for the permeability and porosity of the confining layers (caprock and basement). The latter values were the same as those used in a previous simulation study at this site (Stauffer et al., 2013). Heterogeneous permeability fields were generated using sequential Gaussian simulation. Prior to the risk assessment, we calibrated the permeability field based on a recent pump test (water injection). Because the duration of the pump test was short (3 days) and

permeability values were modest ($\sim 5.9 \times 10^{-14} \text{ m}^2$), pressure propagation was observed only in the vicinity of the injector. Hence, only grid blocks around the injector are sensitive to the objective function which is simply defined by the sum of misfits between observed bottom-hole pressure and simulated bottom-hole pressure at the injector. Although permeabilities at sensitive grid blocks were successfully calibrated, most of the reservoir properties remain uncertain. The sensitive grid blocks adjacent to the well were then used as hard data for the sequential Gaussian simulation (Figure 3-4).

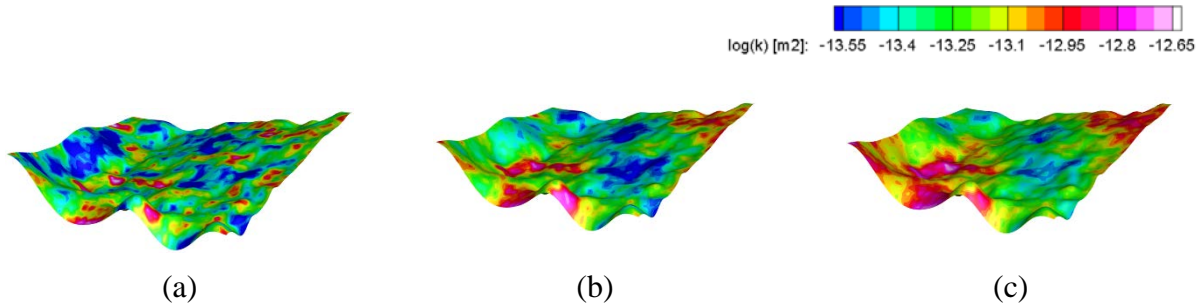


Figure 3-4: Heterogeneous permeability fields (top layer of the injection zone). (a) Correlation length = 1000 (m), (b) Correlation length = 3000 (m), and (c) Correlation length = 5000 (m)

Matrix porosity is set as a constant value (Zhou et al., 2013) for simplification, whereas fracture porosity is computed by a correlation (Bernabe et al., 2003 and Deng et al., 2012) to reduce the number of parameters.

$$k = a\phi^b \quad (5)$$

where, k is permeability (m^2), ϕ is porosity, a and b are constants depending on different processes and materials. In this study, $a = 5.92 \times 10^{-7}$ and $b = 3.0$ (Deng et al., 2012)

Relative permeability curves used in the sensitivity analysis are presented in Figure 3-5. Yoshida et al. (2016) conducted a robust, statistical sensitivity analysis of relative permeability parameter values in CO_2 storage and concluded that total CO_2 injected (bottom-hole pressure constrained) is statistically correlated to only the end-point CO_2 relative permeability. Hence, we only use the end-point CO_2 relative permeability as an uncertain parameter for relative permeability curves although the Corey equations have other parameters such as exponents and residual saturation.

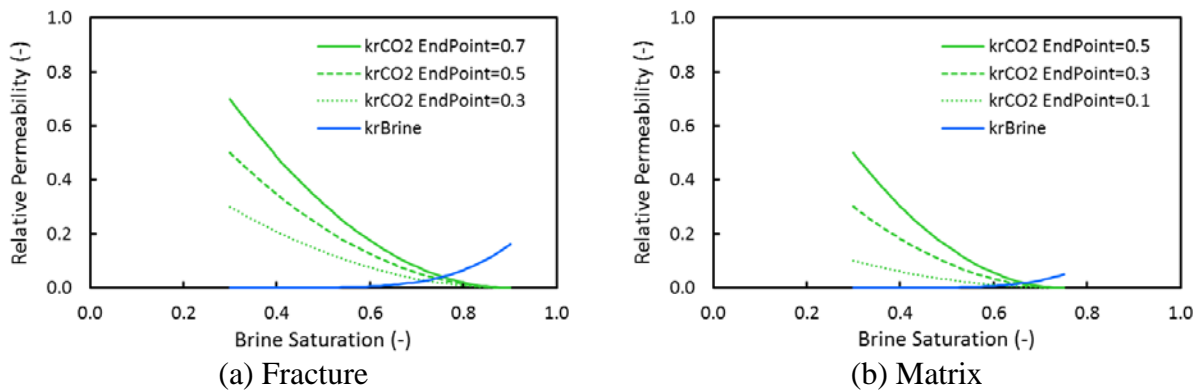


Figure 3-5: Relative permeability curves

Relative permeability hysteresis was also considered. Different relative permeability curves were used for the drainage and imbibition processes (Juanes et al., 2006). Several empirical models to describe hysteresis effects have been developed (Land, 1968; Killough, 1976; Carlson, 1981). We used the Land model in this study:

$$S_{CO_2,t} = \frac{S_{CO_2,i}}{1.0 + CS_{CO_2,i}} \quad (6)$$

And,

$$C = \frac{1.0}{S_{CO_2,t,max}} - \frac{1.0}{S_{CO_2,max}} \quad (7)$$

where, $S_{CO_2,i}$ is the initial CO_2 saturation (CO_2 saturation at flow reversal), C is the Land trapping coefficient, $S_{CO_2,max}$ is the maximum CO_2 saturation and $S_{CO_2,t,max}$ is the maximum trapped gas saturation. The Killough's method was applied for scanning curves (Killough, 1976). The Land trapping coefficient was set at 1.0 (Juanes et al., 2006) because parameters in Equation (7) are unknown. We used the range for Land trapping coefficient between the values $0.2 < C < 5.0$ (Krevor et al., 2015). The implication of C is illustrated in **Figure 3-6**. Higher C indicates less trapping (i.e., similar drainage and imbibition curves), and vice versa.

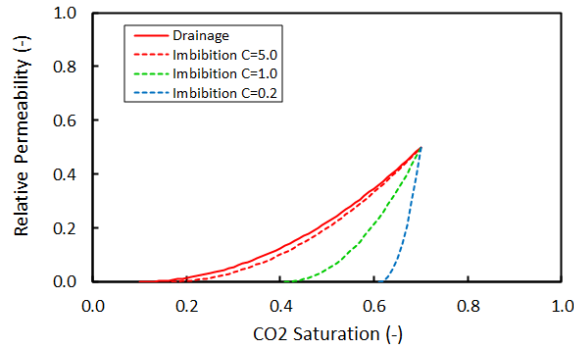


Figure 3-6: Hysteresis relative permeability curves

Figure 3-7 presents all the quantities for fracture CO_2 relative permeability hysteresis. We found that hysteresis of matrix relative permeability did not significantly influence the results and thus is not further discussed in this study.

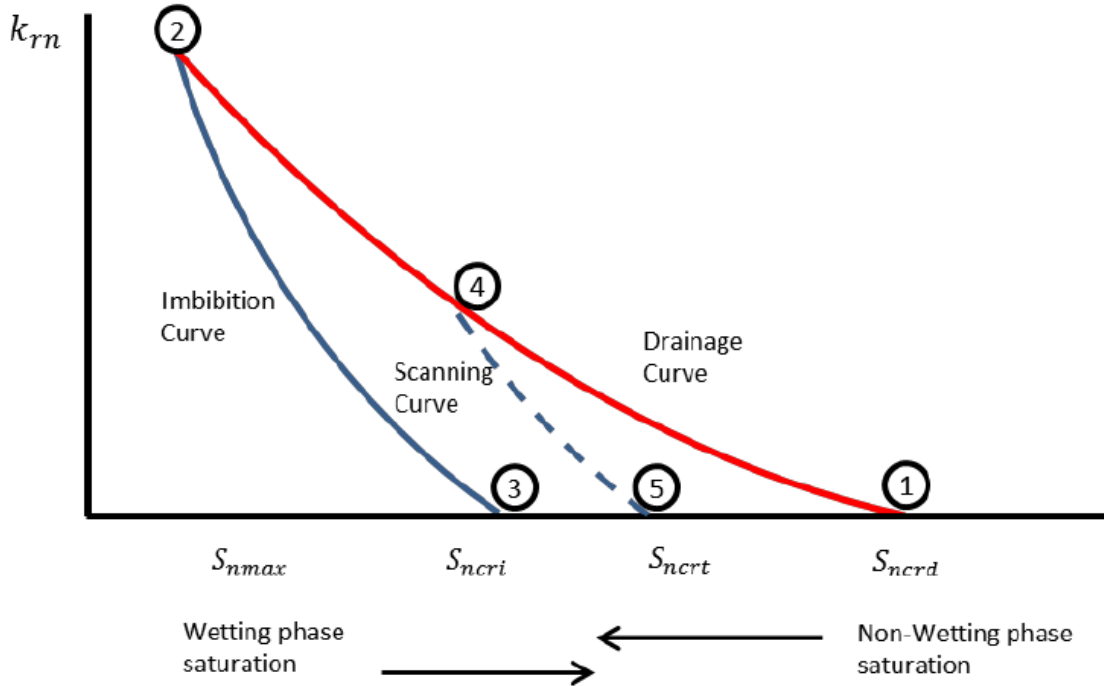


Figure 3-7: Hysteresis of CO₂ relative permeability in fracture (after Schlumberger, 2015)

Capillary pressure plays an important role in CO₂ storage. When CO₂ is injected into a saline aquifer, it will displace the resident fluid (brine) and migrate in response to buoyancy and pressure gradients. Subsequently, the brine imbibes back into the pore space pursuant to the migrating CO₂ plume. Small isolated blobs of CO₂ will be trapped by capillary forces, i.e., capillary trapping or residual trapping (Krevor et al., 2015), which is an important process for maximizing capacity and ensuring the integrity of CO₂ storage. The strength coefficient in Equation (3) was used to explore sensitivity of capillary pressure curves (**Figure 3-8**). Parameter values and ranges are based on Zhou et al. (2013) and Pruess and Garcia (2002) in **Table 2**.

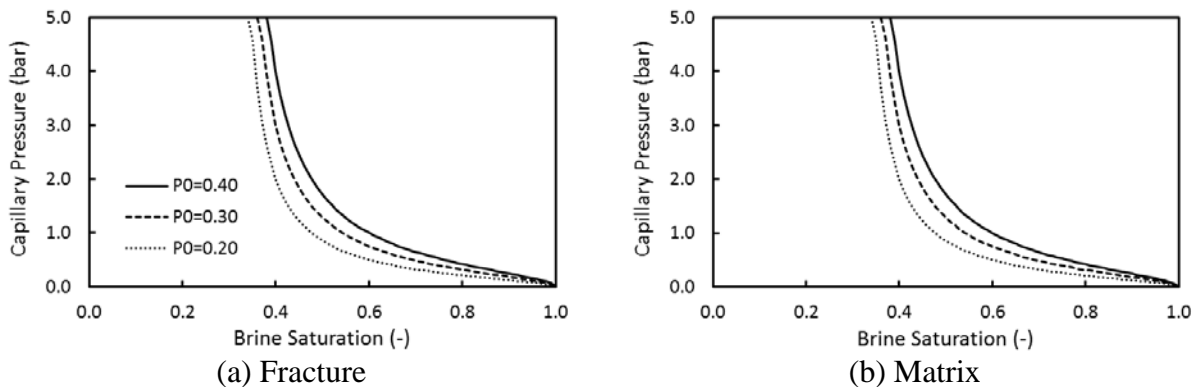


Figure 3-8: Capillary pressure curves in fracture and matrix

The governing equations of the dual-porosity/dual permeability model has an additional source/sink term called the transfer function to address fracture-matrix interactions. The transfer function is proportional to a geometrical shape factor σ (m⁻²), and the driving force is the pressure

drop between a matrix grid block and surrounding fractures. A variety of formulations of the transfer function have been proposed (Warren and Root, 1963; Kazemi et al., 1976; Lim and Aziz, 1995). We applied the commonly used approach assuming pseudo steady-state flow between fracture and matrix domain suggested by Kazemi et al. (1976):

$$\sigma = 4.0 \left(\frac{1}{l_x^2} + \frac{1}{l_y^2} + \frac{1}{l_z^2} \right) \quad (8)$$

where l_x , l_y , and l_z are the distances (m) between fractures in the x, y, and z directions. Because data for fracture distributions are not available, we applied a constant shape factor (σ) value of 0.12 to the entire fracture domain in our lower-end scenario based on Fakcharoenphol et al. (2014). A complete list of sigma values is presented in **Table 3**.

Salinity of the aquifer can affect solubility trapping (Barrufet et al., 2010). The salinity range in this study is based on NETL (2015) and Zhou et al. (2013). Because this is a hypothetical risk assessment, we are not using measured USDW salinity values observed within the Middle Duperow in the Wallewein 22-1 well, where salinity below 10^4 mg/kg was observed.

In our approach, we have 12 parameters (11 parameters have low, base, and high values and hysteresis of CO₂ relative permeability in fractures is on or off) as shown in **Table 3** and therefore we ran 24 reservoir simulations to obtain sensitivities. Subsequently, we applied RROM-Gen and NRAP-IAM to each case and computed CO₂ and brine leakages. As mentioned, permeability and porosity of shallow formations and quality of cements of legacy wells are unknown. To conduct fair comparisons in the sensitivity analysis, typical constant values (Rathbun and Tai, 1988) are used (**Table 4**).

TABLE 4: Parameters for NRAP-IAM

Parameter	Values
Sunburst	
Thickness, (m)	30.0
Permeability, (m ²)	9.9e-14
Porosity, (-)	0.15
Madison	
Thickness, (m)	240.0
Permeability, (m ²)	1.5e-13
Porosity, (-)	0.15
Banff	
Thickness, (m)	30.0
Permeability, (m ²)	9.9e-14
Porosity, (-)	0.15
Wells	
Number of wells in the injection zone, (-)	5
Number of wells in shallow formations, (-)	45
Wellbore cement effective permeability, (m ²)	5.0e-11

For all scenarios in the sensitivity analysis, the sensitivity of parameter i was computed as the difference in the sum of leakage rates normalized by the standard deviations:

$$Sensitivity = \frac{Leakage\ Rate_{l,i} - Leakage\ Rate_{l,base}}{\sigma_l} \quad (9)$$

where l represents different leakage locations of CO₂ and brine to intermediate reservoirs, shallow aquifers, and the atmosphere.

3.2. NRAP-IAM Model

To conduct the risk assessment, we extracted numerical simulation results at each time-step for the top layer in the injection zone which has the highest CO₂ concentrations and used this layer as the source of potential CO₂ leakage. **Fig 3-8** illustrates the workflow of RROM-Gen for a single realization. Note that we only extracted simulation results from the fracture system of the dual-porosity and dual-permeability model as input to NRAP-IAM. The reason is that fractures are where most of the CO₂ flow occurs.

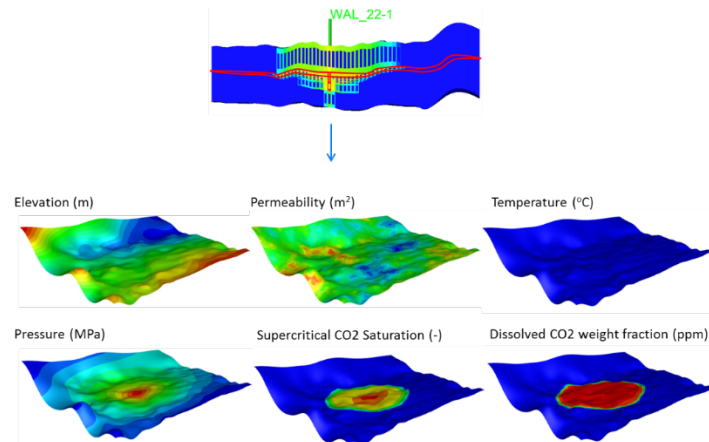


Figure 3-9: RROM-Gen extracted ROMs including elevation, fracture permeability, temperature, pressure, supercritical CO₂ saturation, and dissolved CO₂ weight fraction

The regional geology includes permeable shallow formations (sandstone and dolomitic limestone) where CO₂ or brine could accumulate from a potential leak (**Figure 3-9a**). The Madison formation in **Figure 3-9a** is a known USDW in some locations regionally. In addition, there are 5 legacy wells that penetrate the injection zone and approximately 45 wells that penetrate the shallow formations (**Figure 3-9b**). Unfortunately, permeability and porosity of the shallow formations and wellbore integrity (i.e., permeability of the external annulus) of legacy wells are unknown. We integrated these data into NRAP-IAM and evaluated leakage risks. Each Monte-Carlo realization simulated performance of the CO₂ storage site over 104 years, which include 4 years of CO₂ injection with BHP control and 100 years post-injection relaxation.

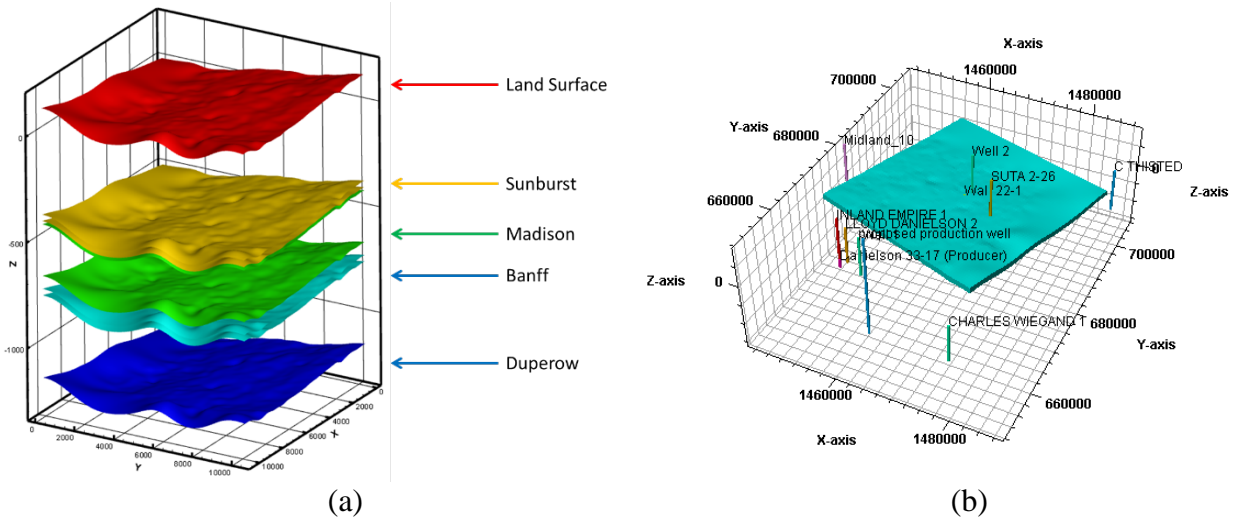


Figure 3-10: Shallow permeable formations and legacy well locations. (a) shallow permeable formations (b) legacy well locations

3.2.1. Model Description

The reservoir simulation outputs including elevation, permeability, temperature, pressure, and CO₂ concentrations were converted into ROMs for NRAP-IAM using RROM-Gen for all realizations. These ROMs were used in NRAP-IAM to calculate leakage processes through two major leakage pathways: legacy wells (Onishi et al., 2017) and faults (Nguyen et al., 2017c).

Input Data – Land Surface

**Land Surface
Temperature (°C)**

**Mass fraction of CO₂
leaving from top layer**

**Geothermal Gradient
(°C/km)**

**Land Surface
Elevation above mean
sea-level (m)**

10

**Wind Speed at 10m above
land surface**

1. m/s

Ambient Temperature

20 °C

Ambient Pressure

1 atm

Leaked Gas Temperature

20 °C

Threshold Concentration

0.002

**Number of Checking Point(s)*
(if CO₂ Concentration is above
Critical)**

7

*(Note: a file named "CheckPoints_CO2concentration.txt"
is needed to define the receptors' locations)

Figure 3-11: The NRAP-IAM input panel for surface parameters.

Input Data – Shallow Aquifer

<u>Hydrologic</u>	<u>Single</u>	<u>Distribution</u>			
		<u>Mean</u>	<u>Std. Dev.</u>	<u>Min</u>	<u>Max</u>
<u>Mean Permeability (Darcy)</u>	<input checked="" type="checkbox"/> Uniform	0.631	1	0.01585	25.12
<u>Permeability Variance</u>	<input checked="" type="checkbox"/> Uniform	0.9535	0.56	0.017	1.89
<u>Permeability Correlation Length (km)</u>	<input checked="" type="checkbox"/> Uniform	2.475	0.87	1	3.95
<u>Permeability Anisotropy (Kx/Kz)</u>	<input checked="" type="checkbox"/> Uniform	25.1	14.4	1.1	49.1
<u>Aquifer Thickness (m)</u>	<input checked="" type="checkbox"/> Uniform	300	120	100	500
<u>Horizontal Hydraulic Gradient</u>	<input checked="" type="checkbox"/> Uniform	0.009594	0.00558	0.000288	0.0189

Figure 3-12: The NRAP-IAM input panel for shallow aquifer statistical parameters.

3.2.1.1. Wellbore Input Parameters

CO₂/brine leakage to the atmosphere, shallow groundwater aquifers, and an intermediate reservoir through abandoned wellbore pathways was calculated from the wellbore leakage ROM (Harp et al. 2016). There are 5 legacy wells in this study and their location was imported as shown in **Figure 3-12**. Well cement permeability distributions were taken as the FutureGen high-rate well models given in NRAP-IAM, which specifies a leakage rate of 11,000 tonnes/year at a frequency of one leaking well once in 10⁻³ to 10⁻⁵ well years (Carey, 2017). In this study, only leakage through external cement pathways is considered.

Input Data – Legacy Wells

Number and Location: Multiple Wells with Known Location (input through input file)

Wellbore Type and Permeability: Cemented well - Permeability Distributions

Location of single known well (X, Y)

X (m) Y (m)

Define rectangular domain for placing wells with unknown locations (for randomly placed single or multiple wells)

Xmin (m) Ymin (m)

Xmax (m) Ymax (m)

Number of Wells

Multiple Wells with Known Locations:

Multiple Wells Number Based on User-Defined Spatial Density (wells/km2)

Multiple Wells Number Based on User-Defined Distribution

Mean Min

Std. Deviation Max

Figure 3-13: The NRAP-IAM input panel for defining legacy wells with known locations for well leakage calculation.

This option for wellbore leakage assumes that permeability is constant along the borehole for each well. However, when this leakage option is invoked, the permeability values assigned to wells are chosen from distributions of permeability values. In the current study, permeability values are based on FutureGen high-rate field data of observed leakage along wellbores (Carey, 2017). Next, the IAM tool uses a ROM to calculate leakage of CO₂ into the atmosphere and both CO₂ and brine into two overlying aquifers using (Harp et al., 2016). The leakage module ROM was constructed from 3D wellbore leakage simulations using the FEHM code, which handles multiphase, non-isothermal flow using the control volume finite element method (Zyvoloski, 2007). Latin Hypercube sampling of parameters was used to ensure coverage of the solution space. The FEHM simulations were performed with the assumptions that the wellbores can be modeled using Darcy flow with a continuum porous media simulator. Each wellbore in a NRAP-IAM model is location-specific and has attributes of CO₂ pressure and saturation in the reservoir; these values were used as input to interrogate the ROM to define the rate of CO₂ and brine leakage into each of the overlying aquifers and the atmosphere.

3.2.1.2. Fault Input Parameters

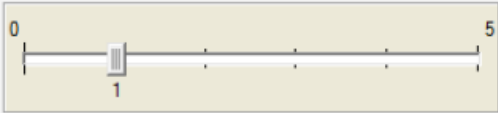
The potential existence of faults at Kevin Dome site provides an excellent opportunity to assess risks associated with hypothetical fault leakage. In this study, the closest fault to Wallewein 22-1 is chosen based on the fault interpretations by Zaluski (2017) to demonstrate the usage of NRAP-IAM workflow (**Figure 2-5**). This fault geometry is modeled using the Fault Swarm model in NRAP-IAM, which employs Monte Carlo (MC) methods.

The fault input data are detailed in **Figure 3-13**. In the interface, one fault swarm is selected from “Number of Fault Swarms”, which allows up to 5 fault swarms to be defined. The input for our

one fault swarm can be done using the “swarm1” column in the input table. Swarm centroid X location, mean and standard deviation (m), specifies an uncertainty range of the swarm centroid location on the X-axis. Likewise, swarm centroid Y location, mean and standard deviation (m), defines an uncertainty range of the swarm centroid location on the Y-axis (**Figure 3-14a**). The input parameters of swarm centroid location set our swarm to the west of Wallewein 22-1 and the injector is at the center of our model domain. Swarm major/minor axis, standard deviation and mean (km), specifies an uncertainty range of the swarm major/minor axis length. Swarm strike, mean and standard deviation (degree), defines an uncertainty range of the spatial orientation of the swarm ellipse from a map view perspective. Fault density, mean and standard deviation (1/km), allows the user to specify an uncertainty range of numbers of individual faults per one kilometer within the swarm ellipse. Fault length, mean and standard deviation (m), defines an uncertainty range of individual fault length within the swarm ellipse (**Figure 3-14a**). Pipe spacing, mean and standard deviation (m), provides an uncertainty range of the leakage pipe spacing along each individual fault (**Figure 3-14a**). Pipe axis length, mean and standard deviation (m), specifies an uncertainty range of pipe axis length in each individual fault. Fault displacement (m) allows the user to specify the individual fault displacements (slip) within the swarm ellipse. Fault displacement increases damage around a fault and leads to increased permeability in the plane of the fault in the NRAP conceptualization. This is discussed in section 3.2.2.2.

Fault Data

Number of Fault Swarms



Fault swarm inputs
(Inputs needed only for the number of swarms defined above.
The input is ignored if number of fault swarms set to zero)

	swarm1	swarm2	swarm3	swarm4	swarm5
Swarm centroid x location (mean) [m]	5258	2000	10000	8000	8000
Swarm centroid x location (stdev) [m]	5	1	100	600	10
Swarm centroid y location (mean) [m]	5258	10000	2000	9000	3000
Swarm centroid y location (stdev) [m]	5	1	100	600	10
Swarm major axis (mean) [km]	2	10	10	15	5
Swarm major axis (stdev) [km]	0	0.1	0.1	1	0.01
Swarm minor axis (mean) [km]	0.5	2	3	1	1
Swarm minor axis (stdev) [km]	0	0.1	0.1	0.5	0.01
Swarm strike (mean) [deg]	90	135	45	180	250
Swarm strike (stdev) [deg]	0	4	10	10	5
Fault density (mean) [1/km]	0.5	2	2	4	3
Fault density (stdev) [1/km]	0	1	1	0.1	0.1
Fault length (mean) [m]	500	3000	2000	400	1000
Fault length (stdev) [m]	3	50	100	40	500
Pipe spacing (mean) [m]	10	500	500	100	200
Pipe spacing (stdev) [m]	1	10	10	10	10
Pipe axis length (mean) [m]	0.2	0.3	0.6	0.4	0.2
Pipe axis length (stdev) [m]	0	0.1	0.3	0.02	0.2
Fault displacement [m]	5000	1333	1300	250	1000

Figure 3-14: NRAP-IAM input panel for fault swarm data.

A fault swarm feature is defined as a group of faults with a resolvable center (centroid) (**Figure 3-14a**). Faults in a swarm share a common mean strike angle, each with a minor angular deviation. Using the statistical input data listed above, an elliptical area in the model domain was randomly populated with individual faults. After each new fault is added, the algorithm performs several investigative walks parallel to the minor axis of the ellipse to determine if the required fault density is satisfied (**Figure 3-14b**). A series of leakage pipes is distributed along the fault plane according to a user-defined spacing parameter, and x-y coordinates are stored for each fault pipe. Any leakage pipe that falls outside the ellipse is subsequently truncated. The remaining pipes are then rotated and translated from the origin to satisfy the swarm geometry parameters (**Figure 3-15**). All pipes that fall outside the model domain following translation and rotation are removed. The spatial distribution of fault swarms, faults, and fault pipes that is generated within the model can be displayed using controls on the *Results - Diagnostics* dashboard of NRAP-IAM.

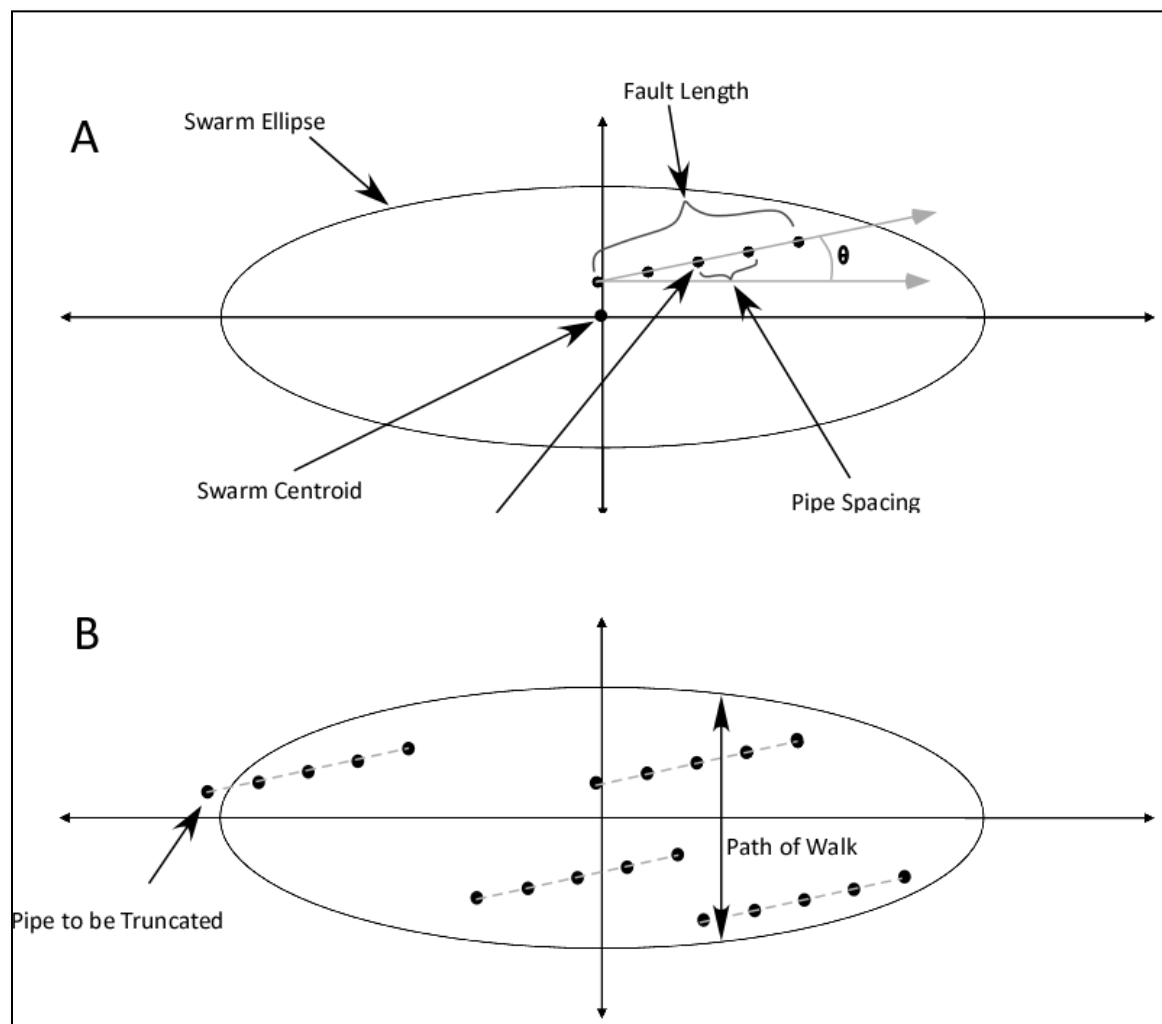


Figure 3-15: Illustration of geometrical construction of faults within a fault swarm ellipse. Major and minor axes of the swarm ellipse lie along the x and y axes, respectively. A) Faults are constructed using fault centroid, fault length, strike angle (θ), and pipe spacing parameter values. B) Multiple faults (and associated pipes) are constructed within the swarm ellipse. The evolving swarm is tested against the fault density parameter (faults per km) by way of a walk parallel to the

ellipse minor axis; if the number of faults intersected exceeds the fault density, then the newest fault is discarded. Finally, the population of pipes in the swarm is truncated by the equation for the swarm ellipse.

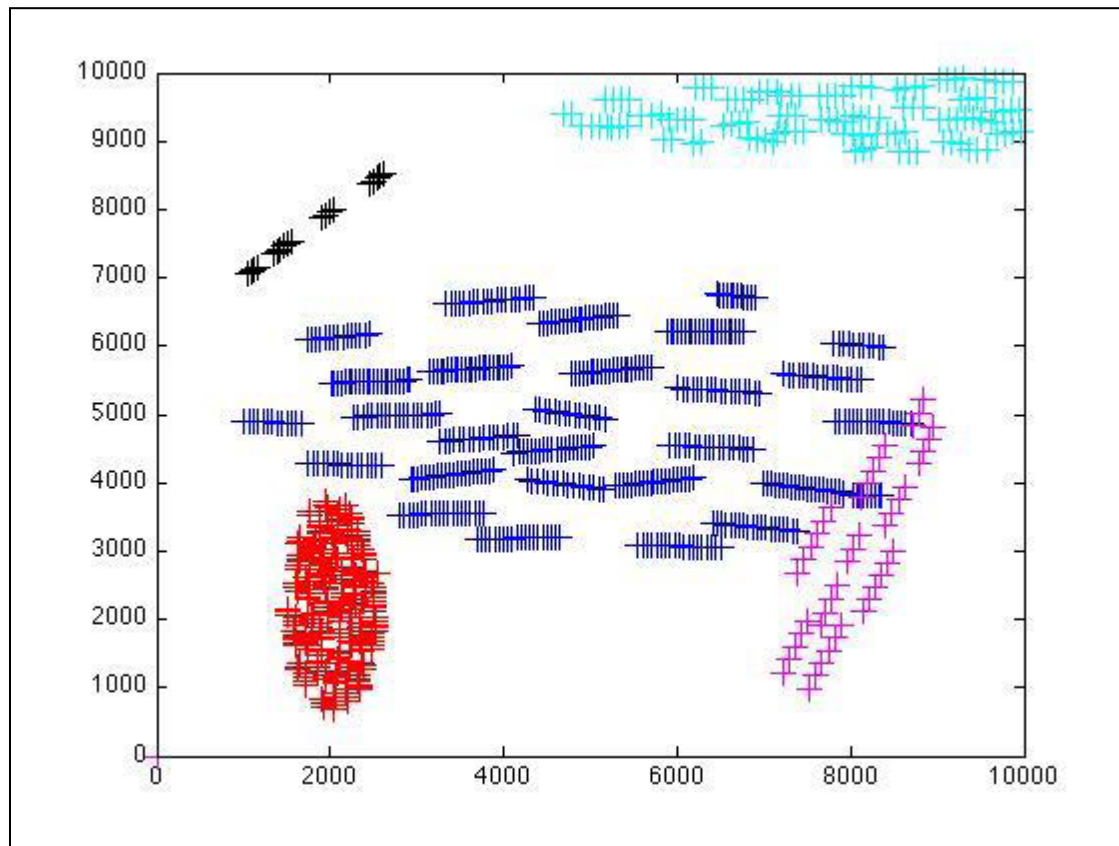


Figure 3-16: Example fault swarms. Plus symbols denote the locations of individual pipes along the length of the fault. The faults have been truncated by the extent of the model domain.

3.2.2. CO₂/Brine Leakage

3.2.2.1. Wellbore Leakage

Five wells penetrate through the injection zone, and 45 wells penetrate the shallow formations. As mentioned previously, permeability and porosity of shallow formations and the wellbore integrity of legacy wells are unknown. We investigated uncertainty of these parameters and fixed the parameter values of **Table 4** for other properties associated with the overlying aquifers.

As described in Section 3.2.1, leakage through wellbore pathways was calculated using ROMs developed by Harp et al. (2016). The wellbore leakage ROM is intended to simulate CO₂ and brine leakage within a cemented wellbore using inputs based on the characteristics of the wellbore and from a dedicated reservoir model without wellbores.

In order to capture the coupled effects of wellbore leakage on pressure and CO₂ saturation within the reservoir, a 3D numerical model that couples the reservoir and wellbore model is used to simulate the fluxes (model responses). This model will be referred to as the “coupled model”. This model was also run without a wellbore in order to collect the pressures and CO₂ saturations at the base of the wellbore consistent with values from a dedicated reservoir model. This model will be referred to as the “reservoir model”.

To capture the coupled effects, some inputs are sampled directly, while other inputs are sampled indirectly using a surrogate parameter. Parameters that are generated through Latin Hypercube Sampling (LHS), a space-filling technique, include:

1. Depth to the bottom of the wellbore (d [m])
2. Cement permeability (k [m²])
3. Injection rate of the CO₂ injectors (q_{CO_2} [kg/s])

Where d and k are directly sampled inputs and q_{CO_2} is a surrogate parameter used to indirectly sample:

1. Log CO₂ saturation at the base of the wellbore from the dedicated reservoir model (SCO_2 [-])
2. Delta pressure (pressure minus initial pressure; $P-P_0$) at the base of the wellbore from the dedicated reservoir model (PCO_2 [MPa])

The model responses collected from the coupled model are:

1. Transient CO₂ flux up *the* wellbore (Q_{CO_2} [kg/s])
2. Transient brine flux up the wellbore (Q_{brine} [kg/s])

A ROM is generated using a Multivariate Adaptive Regression Splines (MARS) algorithm (Friedman, 1991) for each model response: 1) Q_{CO_2} and 2) Q_{brine} .

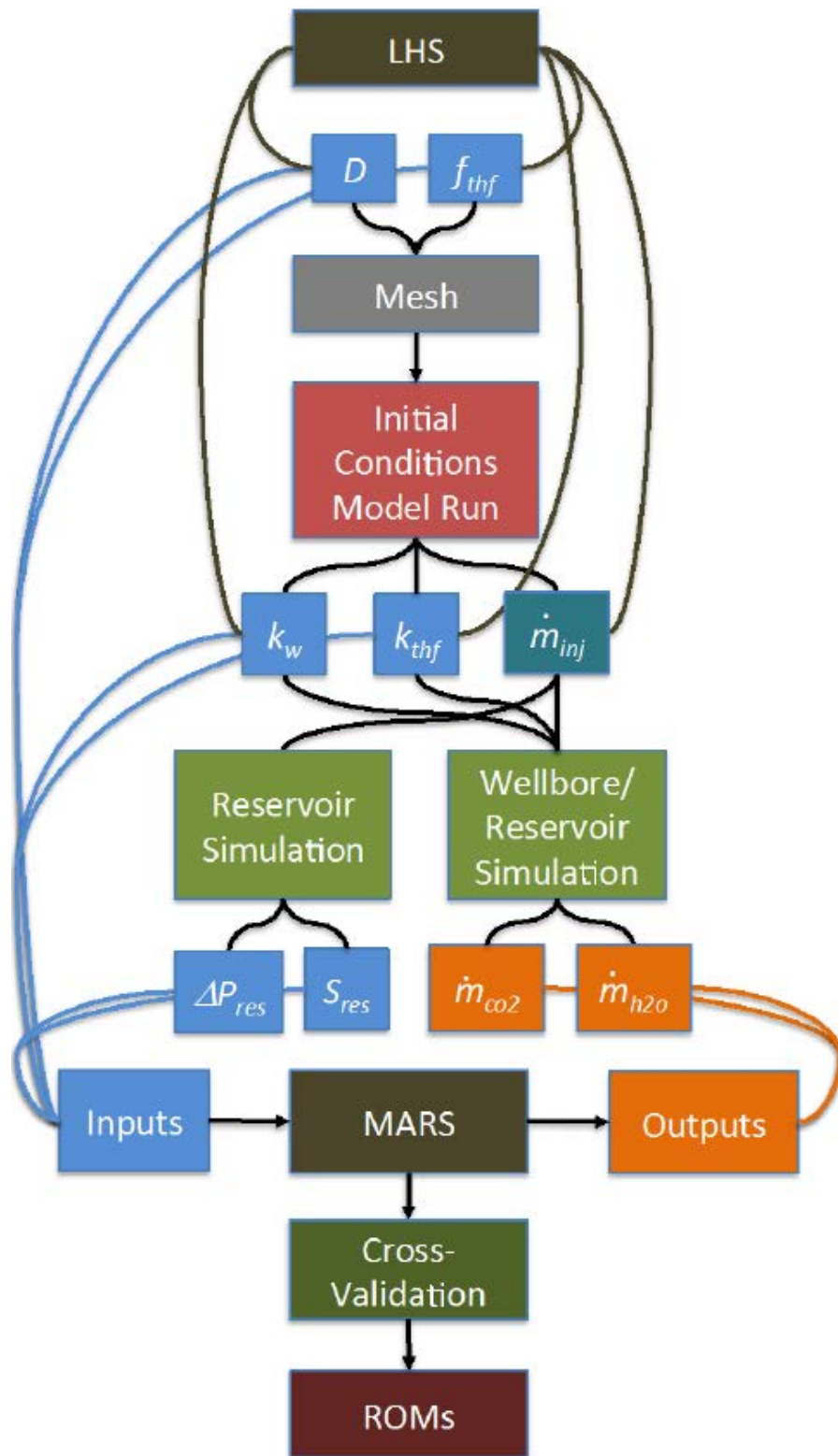


Figure 3-17: ROM development flow diagram (from Harp et al. 2016)

3.2.2.2. Fault Leakage

CO₂ and brine leakage through faults was calculated using LHS sampling of FEHM model results for combinations of thickness and permeability for each aquifer described for leakage along abandoned wellbores.

Flow calculations assume that the fault pipes can be modeled using Darcy flow with a continuum porous media simulator, faults are oriented subvertically, and that fault pipes intersect the reservoir, aquifers, and soil within the same model bin.

Faults have been characterized by the following architectural elements (Caine et al., 1996; Shipton et al., 2002; Shipton et al., 2005):

- *Host rock* (protolith) unaffected by fault
- *Damage zone* containing deformation bands, fractures that slightly decrease host rock permeability perpendicular to the fault plane and may enhance permeability parallel to the fault plane
- *Fault core* (“fault rock”) composed of gouge, cataclasis, and slip surfaces that typically exhibits permeabilities much lower than the host rock.

Sorkhabi and Tsuji (2005) generalized the relationship between host rock and fault in the form of a conceptual rotation of the permeability anisotropy from horizontal in the host rock (due to bedding) to subvertical in the fault zone, enhancing flow parallel to the fault plane.

Spatial variation in the geometry of a fault creates hydrogeologic anisotropy and heterogeneity. The width of the fault zone and its bulk permeability vary along strike and along dip. Although the fault damage zone generally forms a fault-parallel high-permeability zone, fluid flow (water or gas) has been observed to be concentrated in discrete points or small areas along the surface expression of faults, and the subsurface flow is hypothesized to follow higher-flux conduits or pipes (Fairley et al., 2003; Annunziatellis et al., 2008). The spacing for these pipes can be developed from the observed distribution of concentrated flow zones in field sites (**Figure 3-17**).

The fluid flow characteristics of faults also vary through time. Faults may form conduits or pipes for flow during and shortly after seismic activity due to new and open fractures, but with time these pipes may become sealed as a result of mineral precipitation or tectonic processes. However, field studies of natural leaking CO₂ reservoirs demonstrate that fault damage zone fractures through the reservoir caprock can remain open for substantial periods of time and are not self-sealing (Shipton et al., 2005). The ultimate result is that the overall fault zone may represent a high- or low-permeability feature (parallel and perpendicular to the fault).

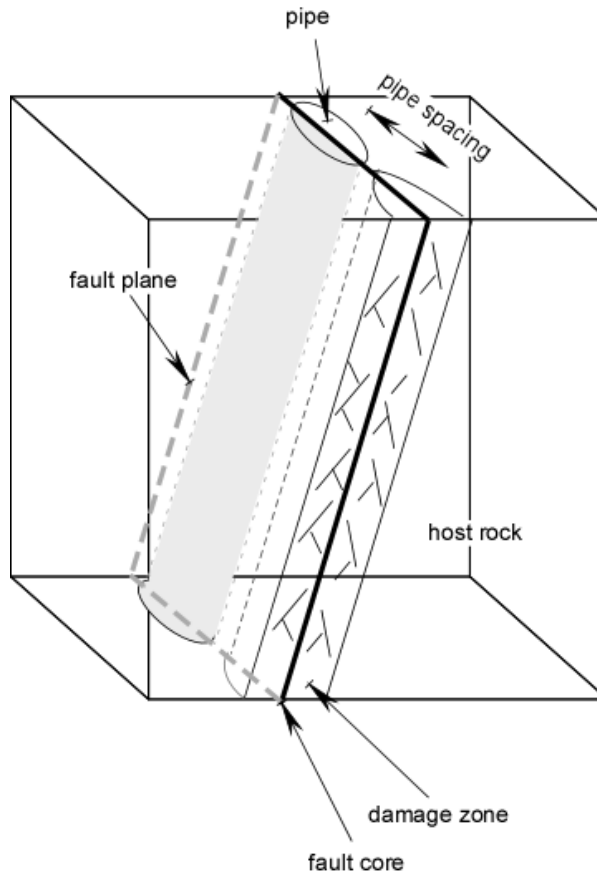


Figure 3-18: Conceptual diagram of the geometrical elements of a fault, including host rock block, subvertical fault plane, fault core and damage zone, and discrete pipes for fluid flow along the fault plane.

Permeability within the fault zone has been measured in sandstone, shale, and granite host rocks but measurements are sparse in carbonates. Most published studies focus on the transverse (fault-perpendicular) permeability as it applies to reservoir compartmentalization. Typical transverse fault permeability, relative to host rock, can be summarized for fault elements as follows (Shipton et al., 2002; Ahmadov et al., 2007; Odling et al., 2004) with k_{hr} being the permeability of undamaged host rock:

Fault core: $k_{fc} = 0.01 \text{ to } 0.1 * k_{hr}$

Slip surface: $k_{sl} = 10 \text{ to } 100 * k_{hr}$

Damage zone: $k_{dz} = 0.01 \text{ to } 0.1 * k_{hr}$

Deformation band (within Damage Zone): $k_{db} = 0.001 * k_{hr}$

Transverse permeability is dominated by the lowest permeability among the fault elements, and generally ranges from

$k_t = 0.001 \text{ to } 1 * k_{hr}$

Transverse permeability is developed in the model as a reduction factor to the host rock permeability, which is conceptually similar to a “skin” factor applied to a well.

Typical *fault-parallel permeability* is dominated by the high permeability of the damage zone (and potentially interconnected fractures—Shipton et al. (2006), and it is characterized by

$$k_p = 2 \text{ to } 1000 * k_{hr}$$

(Sorkhabi and Tsuji, 2005; Ahmadov et al., 2007). Fault-parallel permeability is developed in the model as an enhancement factor to host rock permeability.

The Fault module provides values of CO₂ and brine leakage (kg/day) into aquifers 1, 2, and 3 and into the soil layer for each of the 100x100 spatial bins. These values are used as input to the Aquifer Plume module.

Fault displacement is used to derive width of the damage zone (**Figure 3-17**). The fault permeability models into 3 groundwater aquifers are calculated using this damage zone width value. It is assumed that the width of the near leak flow is 1 km. NRAP-IAM then uses the fault width and transverse fault permeability in a harmonic mean to compute a modified aquifer permeability. This value is fed into the leakage tree in the place of the original aquifer permeability. The following equations describe the relationship:

$$\text{Width of damage zone (m)} = \text{Fault displacement} / 100 \quad (9)$$

$$\text{Fault aquifer 1 permeability model (m}^2\text{)} = 1000.\text{m} / ((1/\text{fault aquifer 1 permeability skin}) * \text{width of damage zone} + (1/\text{fault aquifer 1 permeability}) * (1000\text{m} - \text{width of damage zone})) \quad (10)$$

3.2.3. Convergence

The purpose of this section is to describe how to determine the number of Monte Carlo simulations required in NRAP-IAM to converge to a stable set of results including CO₂ and brine leakages to an intermediate reservoir and shallow groundwater aquifers. NRAP-IAM will randomly sample injection reservoir CO₂ saturation and pressure distributions from 50 ROMs as well as other reservoir properties (above the injection zone in **Figure 1-1**) from various distributions specified in the input section (**Figures 3-11, 3-12, and 3-13**). We then perform incremental numbers of NRAP-IAM simulations in intervals of 100 until the results stabilize.

Error was also calculated for the case of leakage through legacy wells using equation (9) based on an objective function by Olalotiti-Lawal et al. (2017)

$$\text{Error} = \sum_{i=1}^{ntstep} \left[\left\| \frac{P10_{i,j}^{n+1} - P10_{i,j}^n}{\sigma_{P10_j}} \right\| + \left\| \frac{P50_{i,j}^{n+1} - P50_{i,j}^n}{\sigma_{P50_j}} \right\| + \left\| \frac{P90_{i,j}^{n+1} - P90_{i,j}^n}{\sigma_{P90_j}} \right\| \right] \quad (11)$$

Where

P10, P50 and P90 refer to probability percentiles,

j=Cases(CO2 Leakage to IntAq,CO2leakagetoGW,BrineLeakagetoIntAq,BrineLeakagetoGW)
n: number of samples in NRAP-IAM (100 x n)

4. Results and Discussion

The results of the risk assessment process are a large set of simulations that provide a range of answers to the questions: 1) How much CO₂ can be injected in a 4-year period through a single well? 2) How much CO₂ and brine are likely to leak through imperfect wellbores and what proportion leaks to shallow aquifers versus the atmosphere? and 3) How much CO₂ is likely to leak through possible faults? We begin with an analysis of which parameters exert the dominant control on leakage of CO₂ and brine in a sensitivity analysis. We then present results of full-physics reservoir simulations varying the sensitive parameters and used these results to create a ROM for pressure and CO₂ saturation distributions. The ROM was used as input to calculate leakage from wells and faults, and we conclude by discussing the results and the likely suitability of the site for CO₂ storage.

4.1. Sensitivity Analysis

The results of the sensitivity studies are provided in the tornado charts in **Figure 4-1** and **Figure 4-2**. In these figures, the blue and green bars correspond to normalized sensitivity of low and high values of a sensitive parameter respectively on leakage rates. The yellow bars indicate when hysteresis option is turned on and its impact on CO₂/brine leakage. It is obvious that the most significant parameters for CO₂ and brine leakage are fracture permeability, permeability of confining rocks, end-point fracture CO₂ relative permeability, capillary pressure in fracture and matrix, and hysteresis (Onishi et al., 2017). It is apparent that fracture permeability is important. Heterogeneity of permeability distribution was found to be an important parameter in a previous study (Dai et al. 2014). However, the range of average permeability used here is narrow ($3.95\text{e-}14\text{ m}^2$ to $9.87\text{e-}14\text{ m}^2$) according to Zhou et al. (2013), and therefore heterogeneity of permeability has little influence. Permeability of confining rocks controls the amount of CO₂ migration into the caprock during the post injection period and the pressure drop in the injection zone. End-point fracture CO₂ relative permeability is also an important parameter which is consistent with Yoshida et al. (2016). Capillary pressure controls the size of the transition zone between gaseous phase and aqueous phase. In addition, the difference between fracture and matrix capillary pressure affects fracture-matrix flow. According to the Dual Porosity Dual Permeability (DPDP) formulation, when fracture capillary pressure is higher than matrix capillary pressure, more CO₂ migrates into the matrix domain, and vice versa. For example, when more CO₂ flows into the matrix system, the CO₂ plume in fracture system decreases, potentially reducing the CO₂ leakage amount. As a result, capillary pressure is an important parameter. Finally, hysteresis of CO₂ relative permeability in fractures allow more trapping and therefore a CO₂ plume becomes smaller than the case without hysteresis, which results in lower leakage rates (corresponding to negative normalized sensitivity).

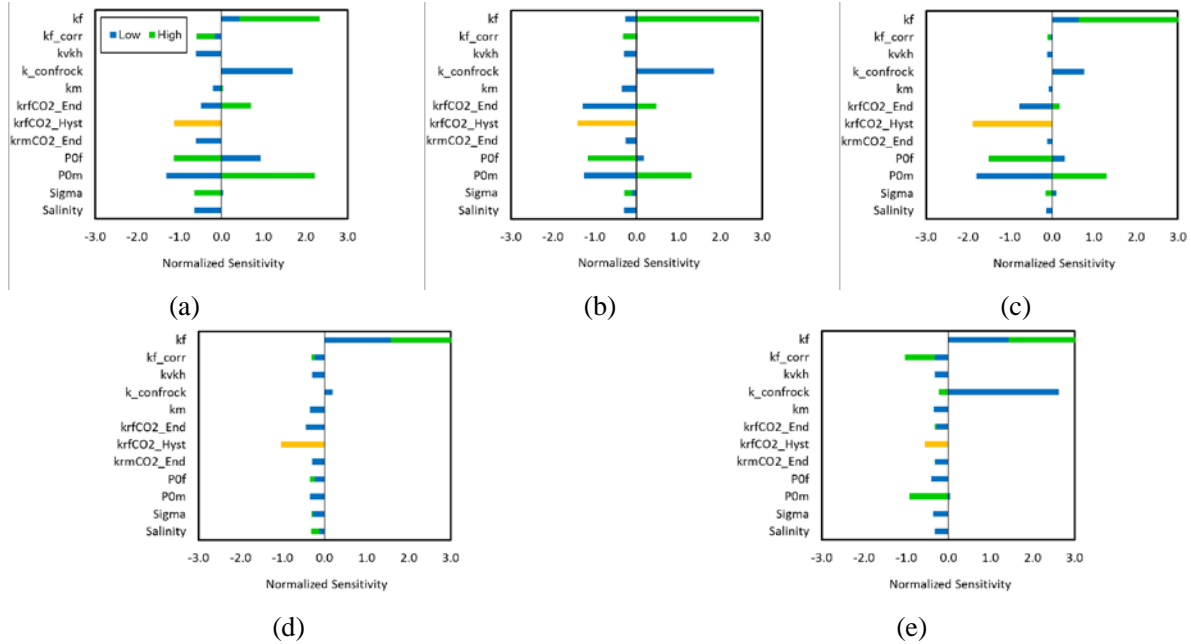


Figure 4-1: Sensitivity analysis results during injection period (4 years). (a) CO₂ leakage to the atmosphere, (b) CO₂ leakage to the intermediate aquifers, (c) CO₂ leakage to the groundwater aquifer, (d) Brine leakage to the intermediate aquifers, (e) Brine leakage to the groundwater aquifer. The yellow bar represents the scenario when hysteresis is turned on.

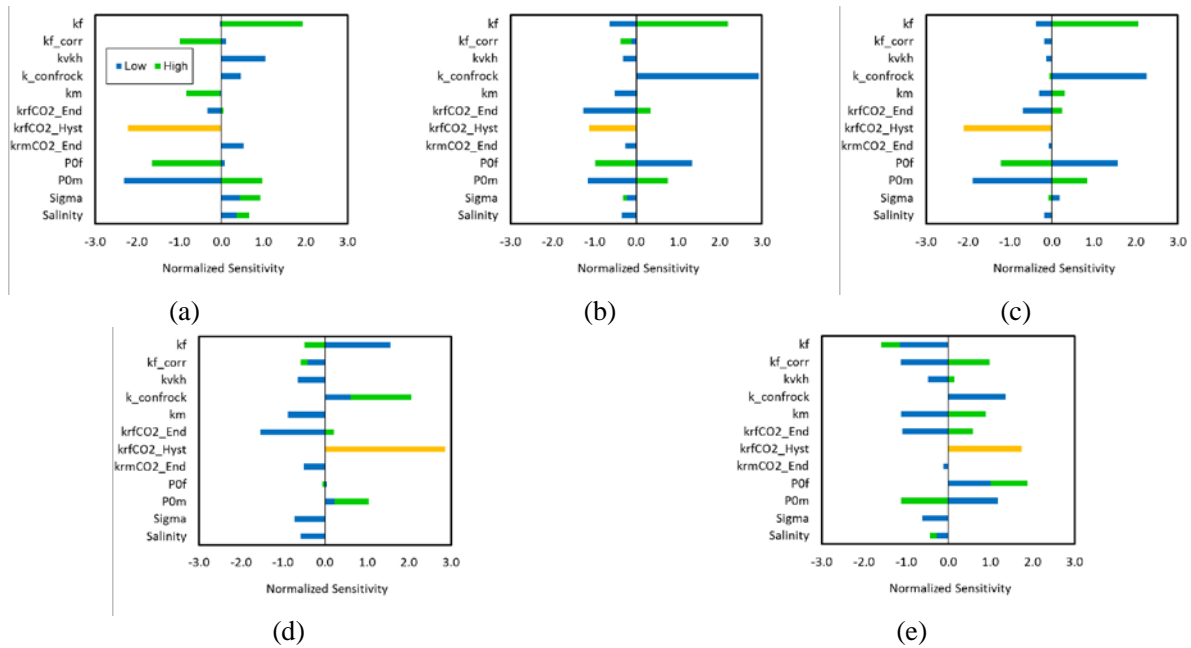


Figure 4-2: Sensitivity analysis results during post-injection period (100 years). (a) CO₂ leakage to the atmosphere, (b) CO₂ leakage to the intermediate aquifers, (c) CO₂ leakage to the groundwater aquifer, (d) Brine leakage to the intermediate aquifers, (e) Brine leakage to the groundwater aquifer. The yellow bar represents the scenario when hysteresis is turned on. See Table 3 for explanation of the parameters.

4.2. Reservoir Simulation

We used LHS to generate 50 realizations for reservoir simulation using the 6 sensitive parameters obtained from the sensitivity analysis. One of the 6 parameters is hysteresis of fracture CO₂ relative permeability, for which we use a constant value in the sensitivity study. **Figure 4-3** presents a cross plot of the correlation between the different parameters sampled by LHS. Small correlation coefficients indicate poor correlations between each parameter, meaning that parameters are efficiently sampled. The distribution of the sampled realizations covers a wide range of uncertainties.

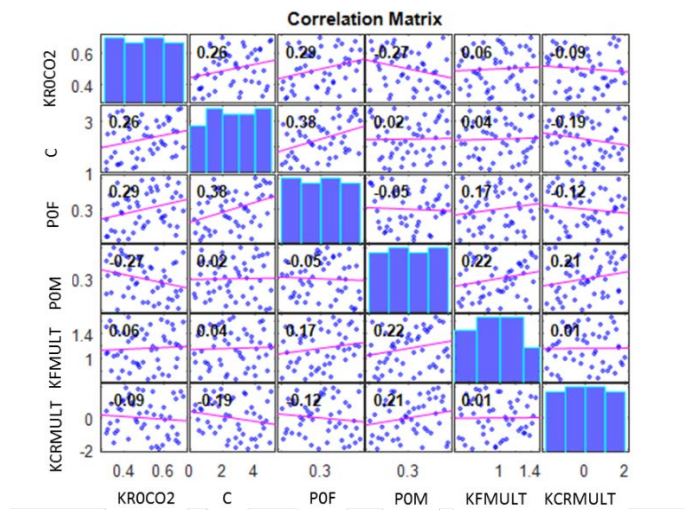


Figure 4-3: LHS results showing correlations among uncertain parameters

The simulation results of total CO₂ injected during four years are overlain on the plot in **Figure 4-4** with P10, P50, and P90 probability values. We found that high permeability, high end-point fracture CO₂ relative permeability, high Land trapping coefficient and low fracture capillary pressure correlate with highest total CO₂ injected. On the other hand, low permeability, low Land trapping coefficient, and high fracture capillary pressure result in low total CO₂ injected. These are consistent with what we have observed from the sensitivity analysis in section 3.1.2. The results also indicate that only about 10% of the simulations inject about 0.75 MT of CO₂ into the middle Duperow, 50% of the simulations inject roughly 0.5 MT of CO₂, and 10% of the simulations inject 0.22 MT of CO₂ over 4 years. These findings show a lower likelihood of successfully injecting 1 MT into the middle Duperow during the four year injection period compared to those reported by Dai et al. (2014), who predicted a greater than 58% probability of 1 MT at the end of 4 years. Dai et al. (2014) borrowed well data from a nearby area which are higher than the fracture permeability used in this study. We consider a wider number of uncertainty parameters (**Table 3**) based on fracture and matrix systems to investigate the total injectivity and leakage potential. These additional parameters, including end point relative permeability of CO₂, hysteresis, capillary pressure, strength coefficient, shape factor and salinity, contributed to the reduction of CO₂ being injected after 4 years.

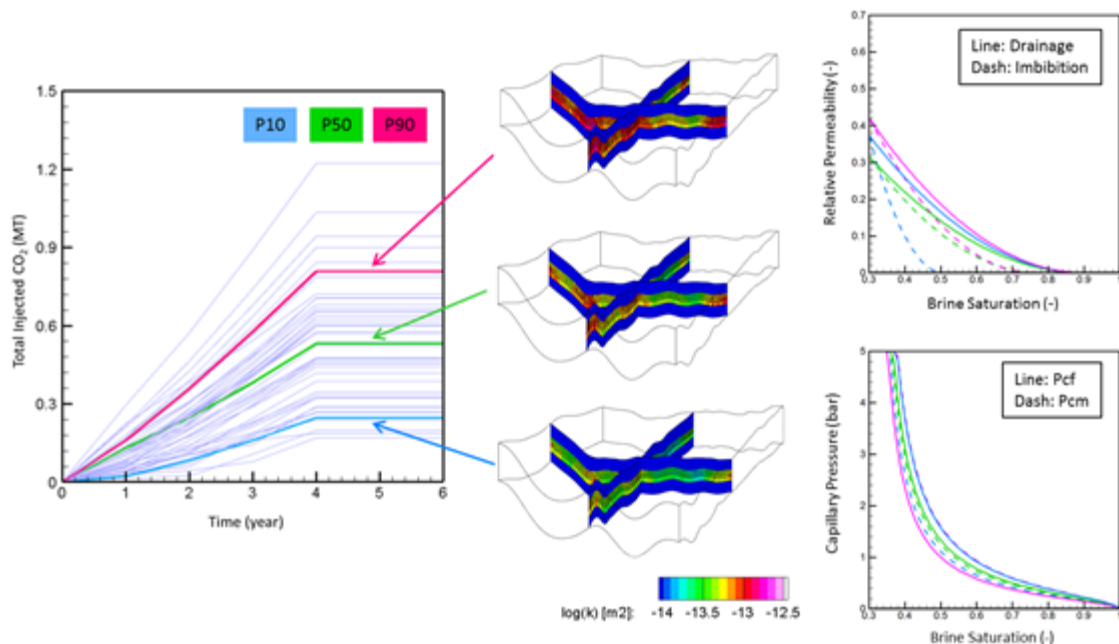


Figure 4-4: Reservoir simulation results including Total CO₂ injection (MT) with P10, P50, and P90 as well as their respective fracture permeability (log(k)) distributions, fracture capillary pressure (Pcf), and matrix capillary pressure (Pcm).

4.3. NRAP-IAM Simulation

We used LHS to sample 50 realizations of reservoir results as an input to NRAP-IAM in order to calculate potential CO₂/brine leakage. Our leakage scenarios include leakage through legacy wells and faults to an intermediate reservoir, three shallow formations and the atmosphere. We investigated i) impact of wellbore cement quality in the event of leakage through legacy wells, ii) impact of fracture permeability, fault length, and fault displacement in the event of fault leakage, and iii) impact of number of samples in NRAP-IAM to converge to stable numerical results.

4.3.1. Wellbore Leakage

Figure 4-5 presents the sensitivity study results (leakage rate in percentage) with varying legacy wellbore cement quality. The majority of OK to very good sealing permeability cases exhibit a leakage rate up to 0.04% of the total injected CO₂ within the first 10 years and then rates decline to around 0.01% or less towards the 50-year mark (total CO₂ injected varies for each realization). Among leaky wellbore (bad to very bad sealing permeability) cases, the leakage rate can go up to 0.18% within the first 10 years and stabilizes down to 0.01% or less toward the end of 50 years. Leakage rates increase the most during the initial 4 years of injection and decline afterwards. Leakage rates appear to stabilize beyond 30 years, regardless of wellbore cement quality. These findings suggest that identifying and locating legacy wells within a reasonable radius of the injector is important in managing all the possible leakage pathways. In addition, monitoring during and post-injection is critical to ensuring CO₂ is contained. On the right hand side of **Figure 4-5** examples are given for the ranges of some of the most important parameters.

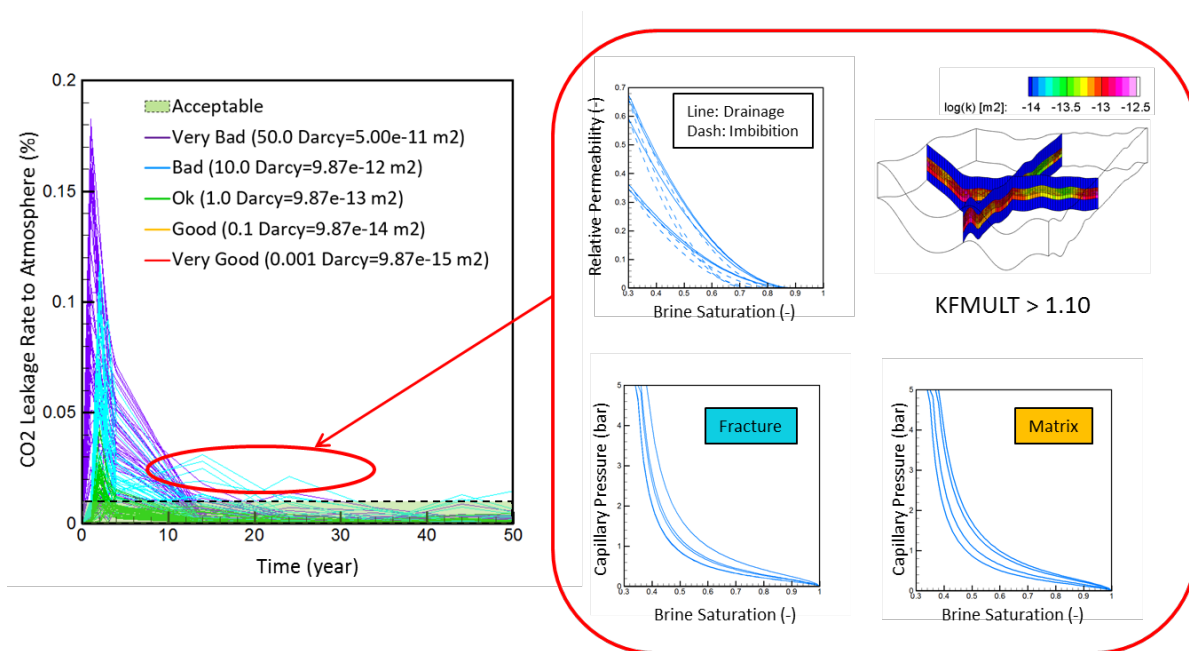


Figure 4-5: Impact of cement quality (shown as Very Bad to Very Good in the legend) on CO₂ leakage to the atmosphere (left panel). The right panel presents parameters (fracture permeability, hysteresis curves, fracture capillary pressure, and matrix capillary pressure) in realizations that result in higher CO₂ leakage.

Another aspect of interest is CO₂/brine leakage rate to an intermediate aquifer and shallow groundwater aquifers. **Figure 4-6** provides a summary of these leakage rates (kg/s) versus time when only the injection period and legacy wellbore leakage are considered. The results indicate that the leakage rates of CO₂ are more sensitive to legacy wellbore cement quality than those of brine. This is partly because of CO₂ buoyancy, which helps it travel upward along a leaky wellbore more easily. It appears that within the first year of injection, almost no amount of brine makes it into the intermediate aquifer from the injection reservoir compared to CO₂. There is, however, seemingly steady leakage of brine from the beginning of injection into shallow groundwater aquifers while the CO₂ leak is relatively small within the same period. This could be explained that due to the proximity of the intermediate aquifer to the surface and groundwater aquifers (**Figure 1-1**), brine could potentially migrate through wellbore leakage pathways and have an impact on USDW. This reinforces the importance of making sure all abandoned wells in the injection area are known before CGS is carried out.

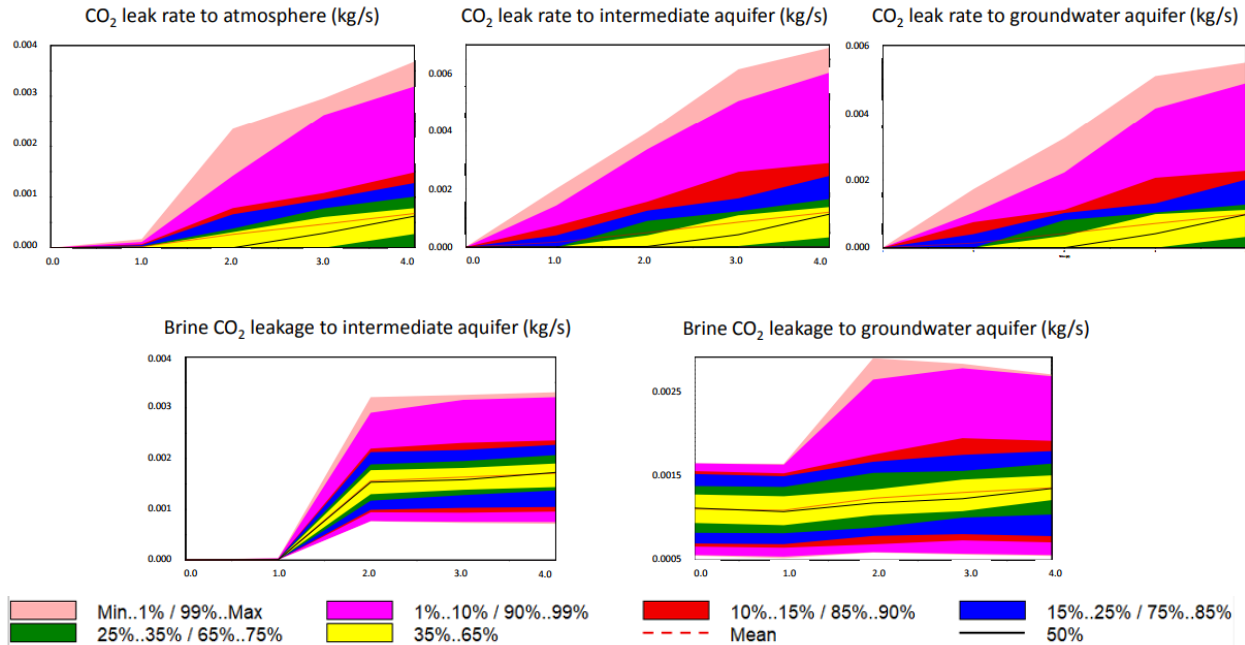
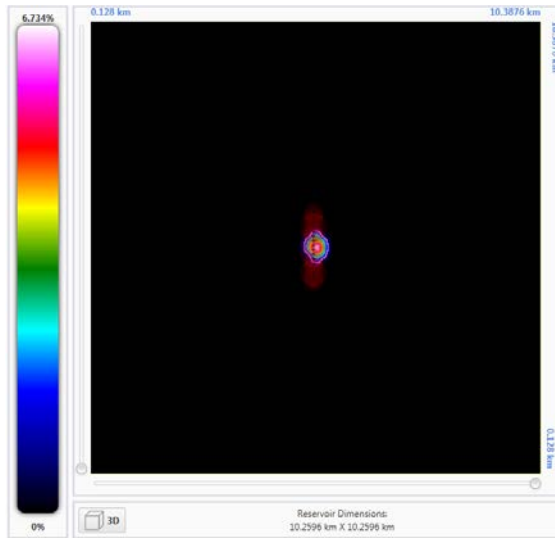


Figure 4-6: CO₂/brine leakage (kg/s) into the atmosphere, intermediate reservoir, and groundwater aquifers versus time (year).

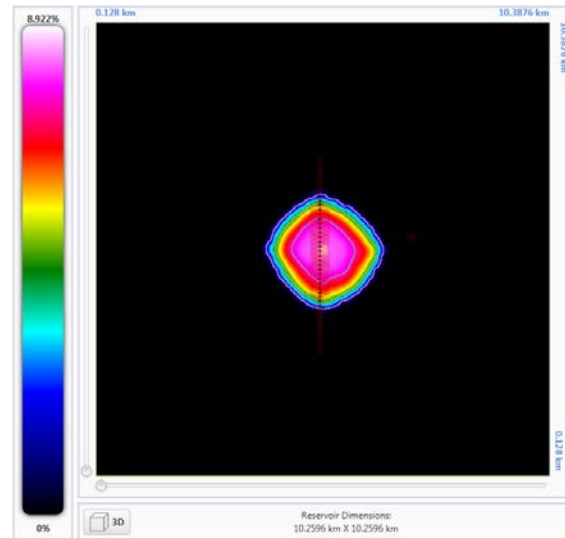
4.3.2. Fault Leakage

In this study, we found that CO₂/brine leakage is sensitive to fracture permeability and fault displacement. Simulation results show that the higher the fracture permeability, the larger the CO₂ plume can become which allows higher chance of CO₂ leakage through fault pathways given the current fault interpretation. Fault displacement is a variable used to increase fault permeability with the assumption that larger slip on faults leads to higher slip plane permeability.

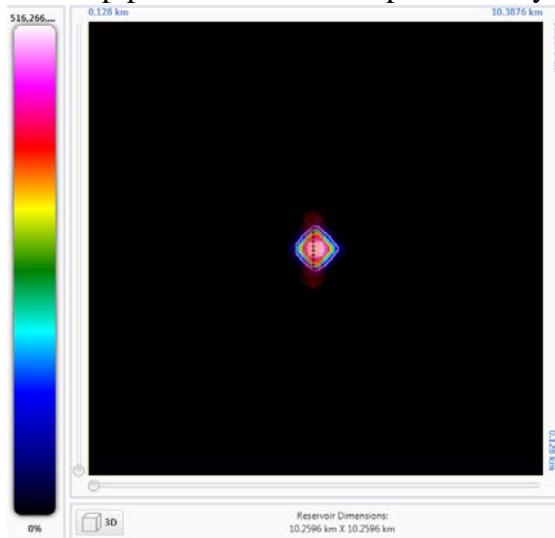
Figure 4-7 depicts a comparison of fault leakage between two cases: low fracture permeability and high fracture permeability. These cases are generated from the base fracture permeability model in **Table 3** using multipliers (0.706 for low and 1.458 for high) to recreate a range of uncertainty. The reason why there is leakage where seemingly no CO₂ saturation exists in **Figures 4-7a** and **4-7b** is the presence of dissolved CO₂ where CO₂ leakage is calculated. In **Figures 4-7c** and **4-7d**, the color scale makes it hard to realize there is dissolved CO₂ saturation since it is very small and is colored black. The color scale in the NRAP viewer could be user-modified in future versions to better delineate the CO₂ plume front. Simulations of these cases exhibit the sensitivity of CO₂ leakage through fault pathways to fracture permeability which makes a significant increase in the total amount of CO₂ leakage (**Figure 4-7e**). Meanwhile, brine leakage is not as sensitive and remains relatively unchanged regardless of fracture permeability (**Figure 4-7f**). However, the amount of brine leakage can be as high as CO₂ leakage if not more (up to 0.0027 MT and above). This suggests that brine leakage could be as significant as CO₂ Leakage.



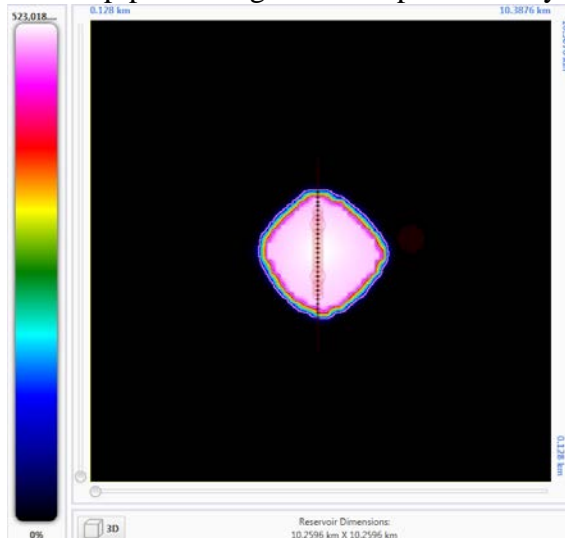
(a) Supercritical CO₂ saturation and leakage nodes/pipes for low fracture permeability



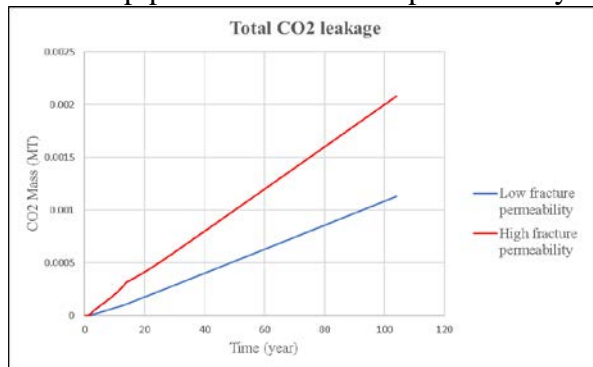
(b) Supercritical CO₂ saturation and leakage nodes/pipes for high fracture permeability



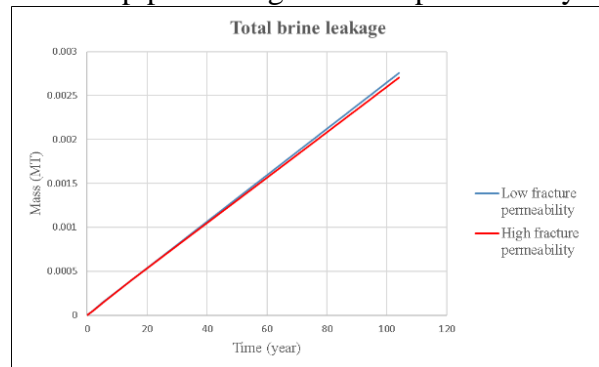
(c) Dissolved CO₂ fraction and leakage nodes/pipes for low fracture permeability



(d) Dissolved CO₂ fraction and leakage nodes/pipes for high fracture permeability



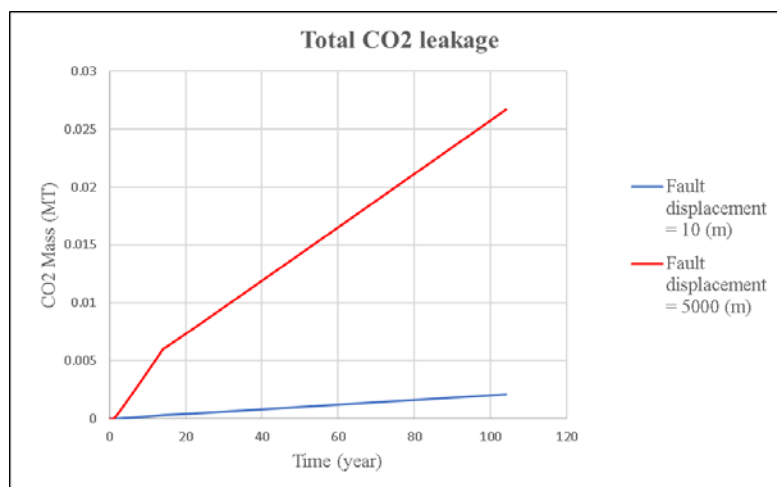
(e) Comparison of total CO₂ leakage



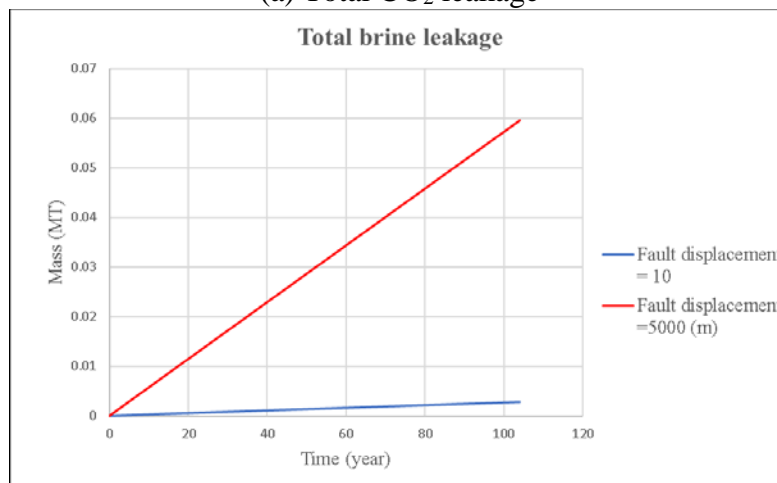
(f) Comparison of total brine leakage

Figure 4-7: Map view of CO₂ plume resulting from leakage from a fault consisting of a series of leakage pipes with low and high fracture permeability cases at the end of 104 years.

Figure 4-8 presents leakage calculation results of low fault displacement (10m) and high fault displacement (5000 m; this value is acting as a tuning parameter and was increased to demonstrate higher leakage in the model. The fault module of the NRAP toolset is still in need of more development). **Figure 4-8a** and **Figure 4-8b** clearly suggest that both CO₂ leakage and brine leakage are sensitive to fault displacement. Under the high fault displacement scenario, CO₂ leakage can go up to 0.025 MT and brine leakage up to 0.06 MT. As for low fault displacement, CO₂ leakage remains well below 0.005 MT and brine leakage well below 0.01 MT. It is important to point out that the vertical extent of fault leakage pathways should be well studied in order to fully understand the risk of CGS into saline aquifers, specifically in the case of the Kevin Dome site. More detailed fault information and interpretation will be obtained from Schlumberger for future study on this project.



(a) Total CO₂ leakage

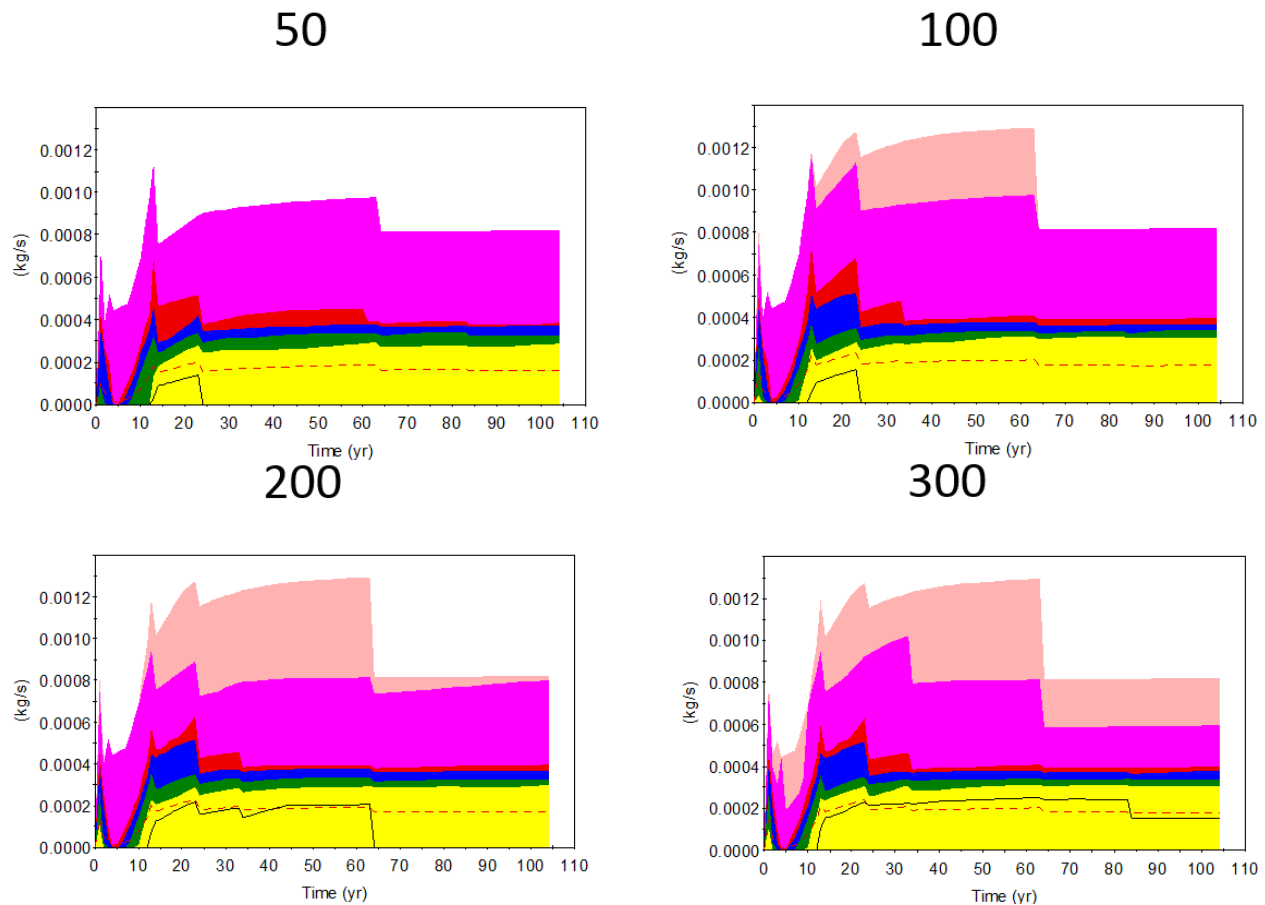


(b) Total brine leakage

Figure 4-8: CO₂ plume and fault leakage of low and high fracture permeability case at the end of 104 years

4.3.3. Convergence

NRAP simulations were carried out to address the convergence issue with Monte Carlo sampling. **Figures 4-9, 4-10, 4-11, 4-12, and 4-13** depict the statistics of CO₂/brine leakage to an intermediate reservoir, groundwater aquifers and the atmosphere. The number on top of each plot in the figures is the amount of simulations carried out during one single run. Since Monte Carlo is a random sampling process, it takes a certain number of simulations to achieve convergence where the results do not significantly contrast from those generated from running a lower number of simulations. This also means that the entire uncertainty distribution domain has been sampled, therefore reaching stable results even if more simulations are performed. Based on these leakage graphs, the Monte Carlo results converge somewhere between 500 to 600 simulations. In the case of broader uncertain parameter ranges or increased number of uncertain parameters, more simulations will be required to cover the uncertainty distributions using random sampling. The time per simulation is substantially reduced due to the use of hybrid (ROMs) instead of full-physics models with NRAP-IAM as an advantage. However, if there is too much uncertainty, LHS may be able to scale down the number of simulations to make it even less computationally expensive while ensuring that the full uncertainty domain is taken into account for.



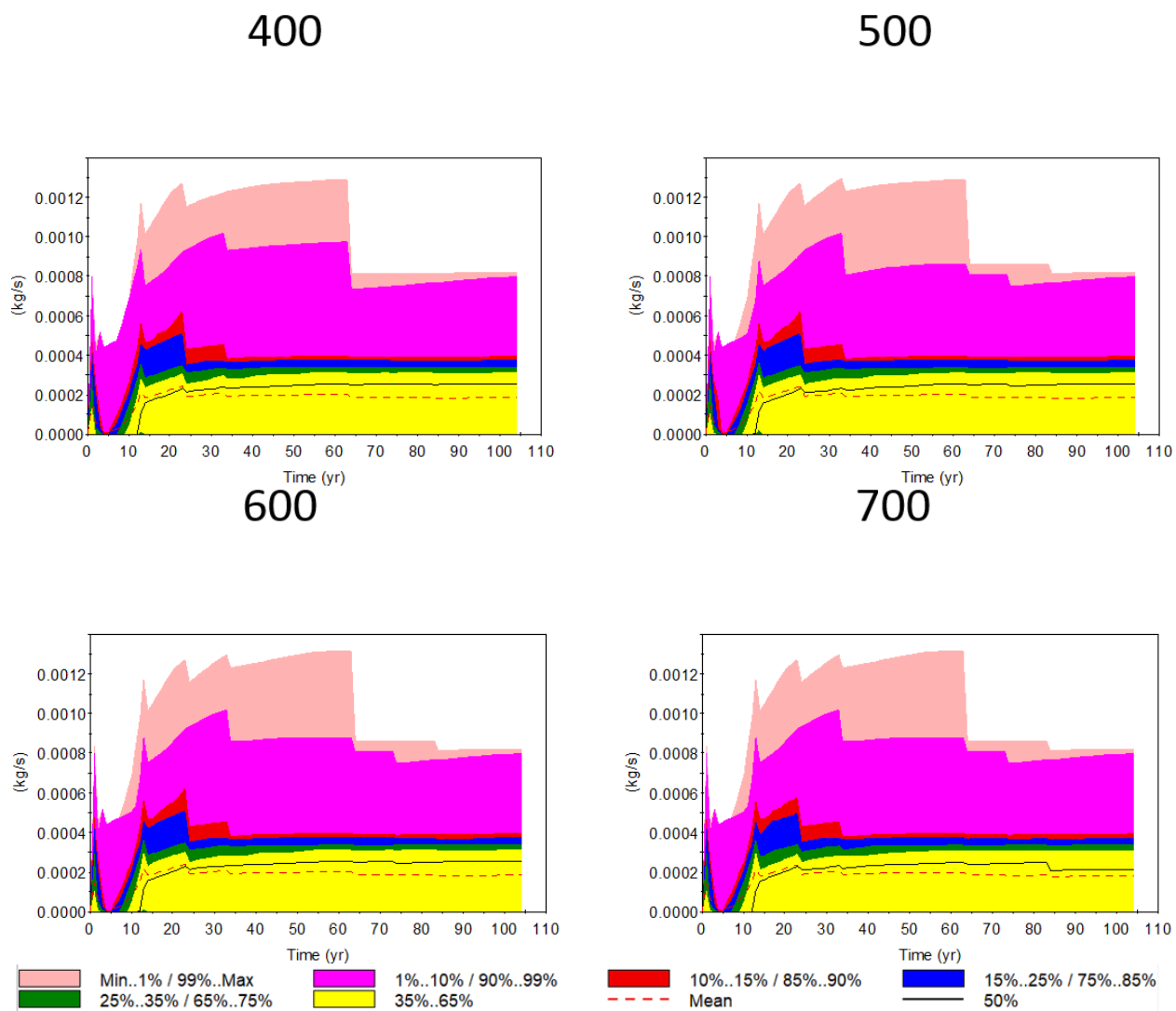
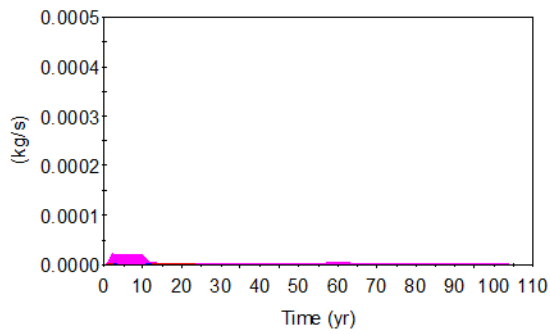
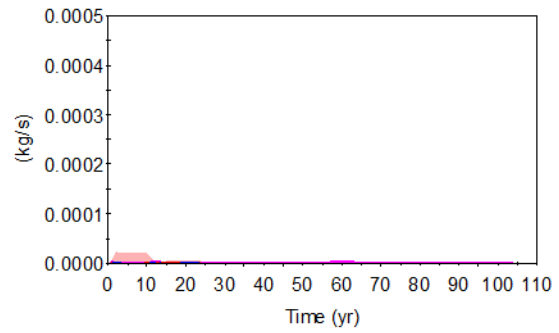


Figure 4-9: CO₂ leakage (kg/s) to an intermediate reservoir over time (year). The numbers on top of each graph represent the amount of NRAP-IAM Monte Carlo simulations performed.

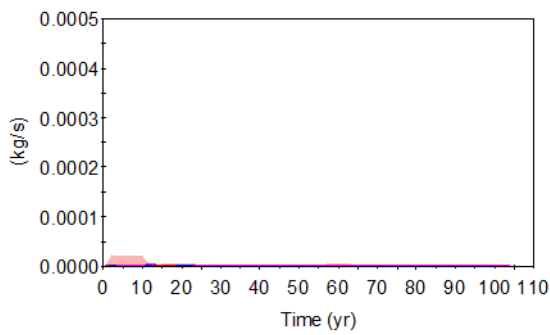
50



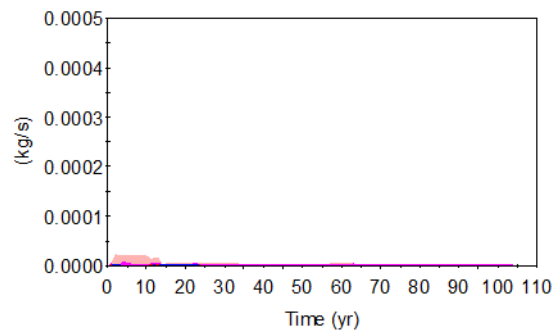
100



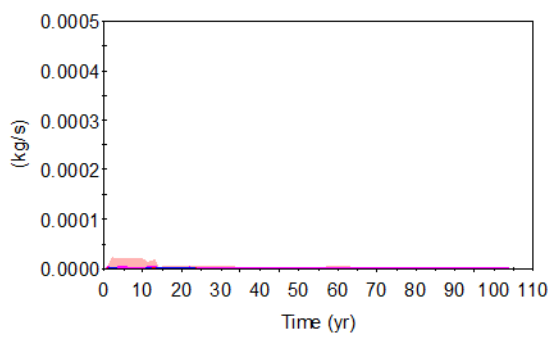
200



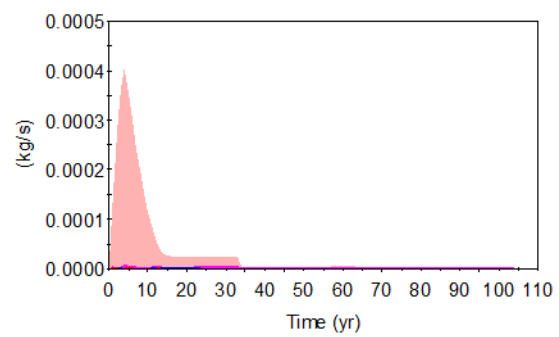
300



400



500



600

700

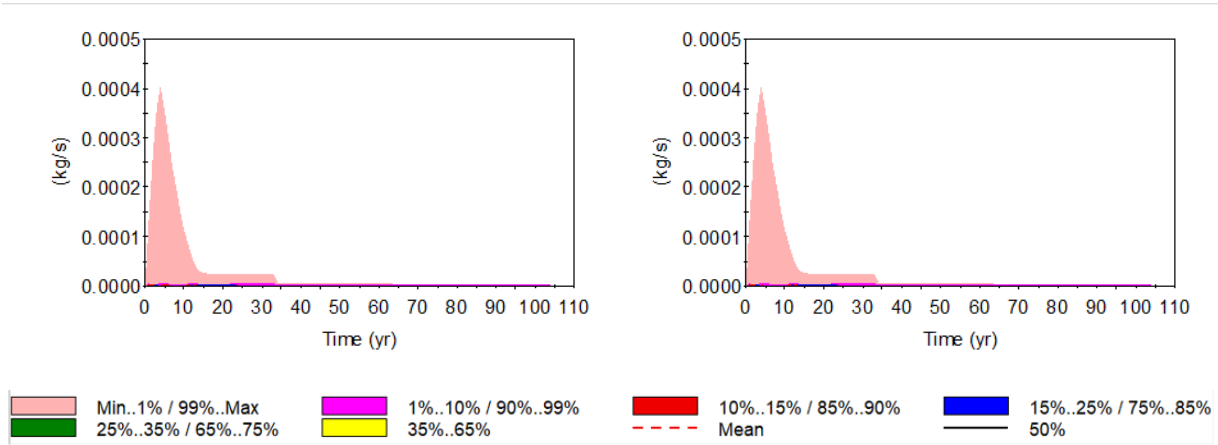
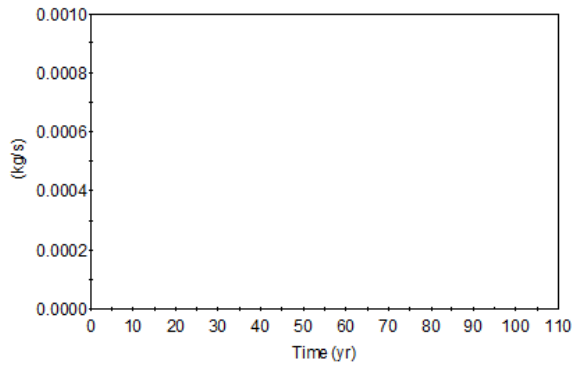
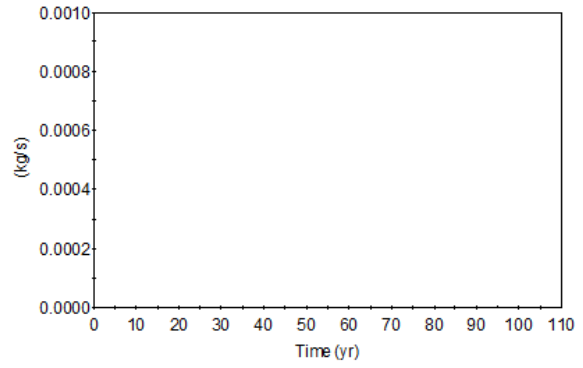


Figure 4-10: CO₂ leakage (kg/s) to groundwater aquifers over time (year). The numbers on top of each graph represent the amount of NRAP-IAM Monte Carlo simulations performed.

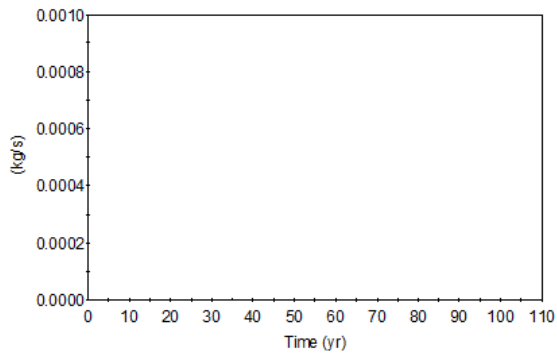
50



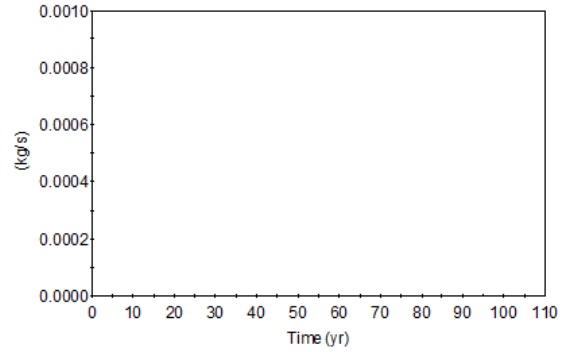
100



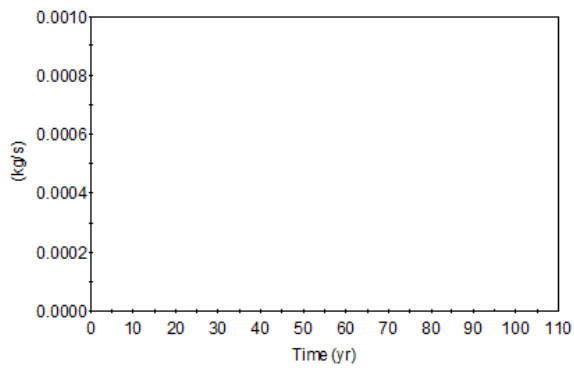
200



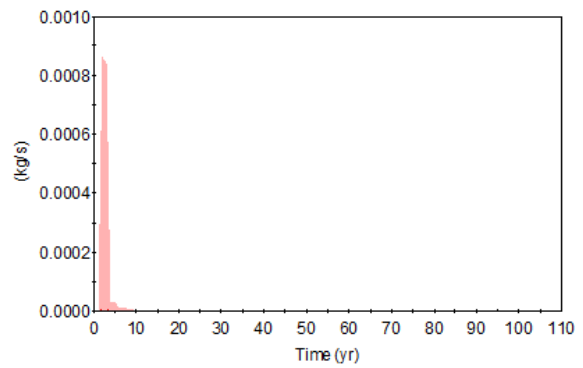
300



400



500



600

700

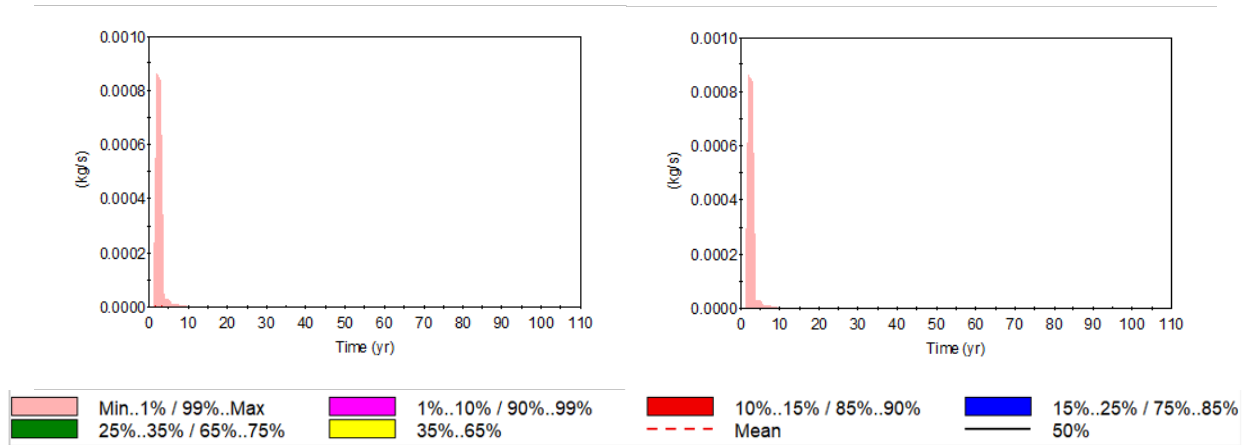
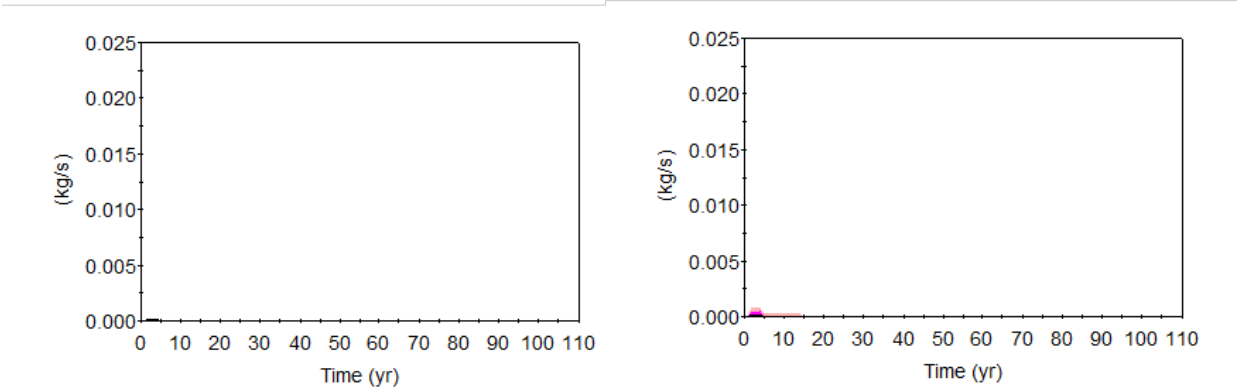


Figure 4-11: CO₂ leakage (kg/s) to the atmosphere over time (year). The numbers on top of each graph represent the amount of NRAP-IAM Monte Carlo simulations performed.

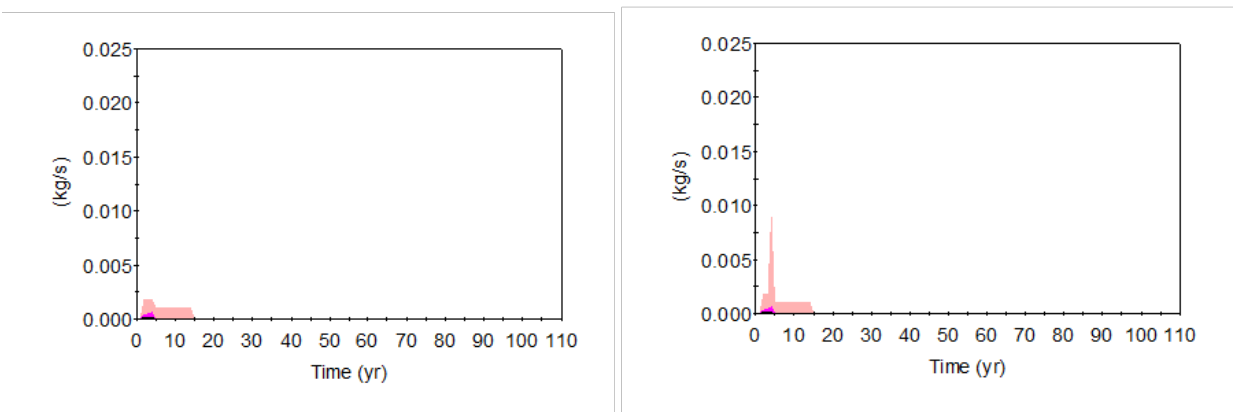
50

100



200

300



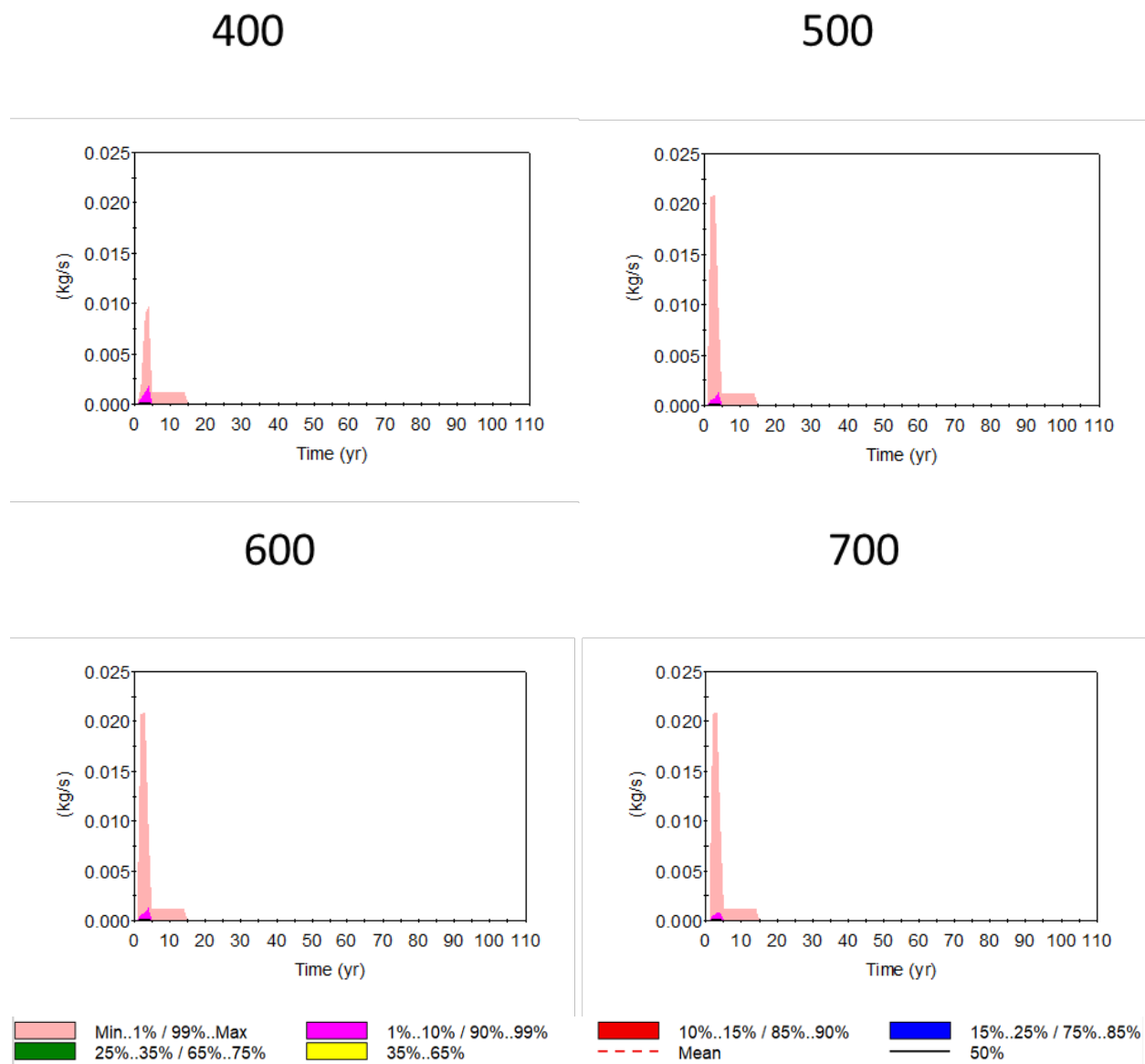
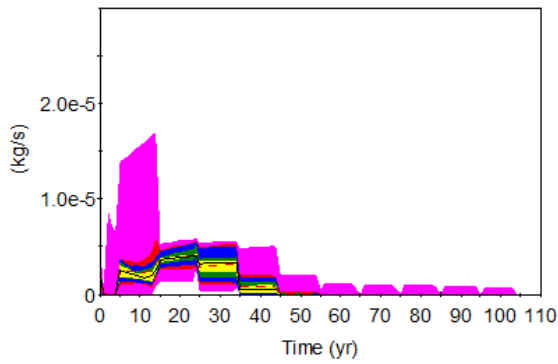
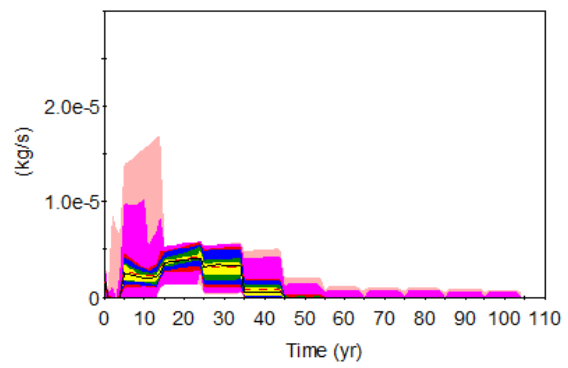


Figure 4-12: Brine leakage (kg/s) to intermediate reservoir over time (year). The numbers on top of each graph represent the amount of NRAP-IAM Monte Carlo simulations performed.

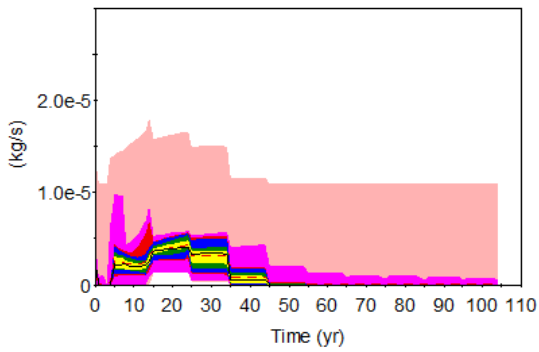
50



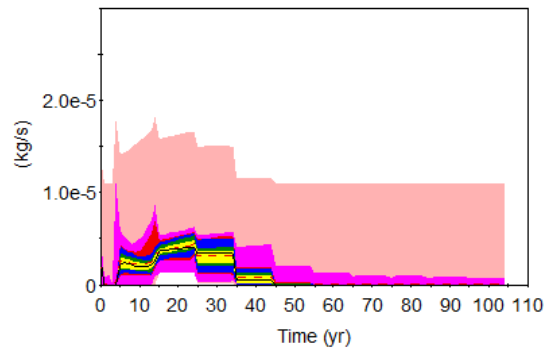
100



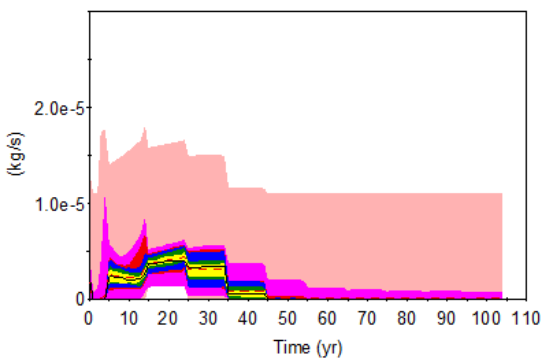
200



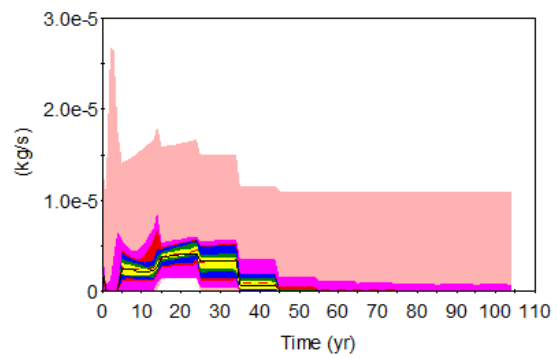
300



400



500



600

700

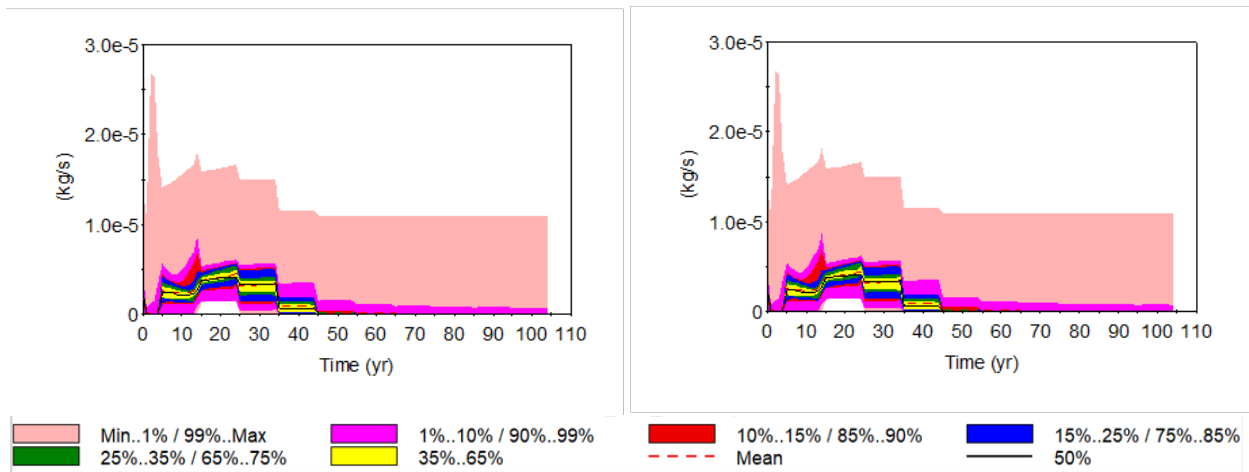
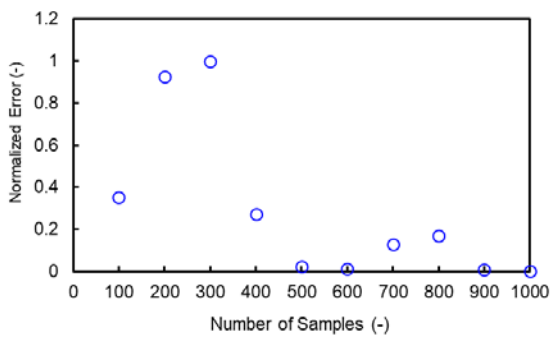
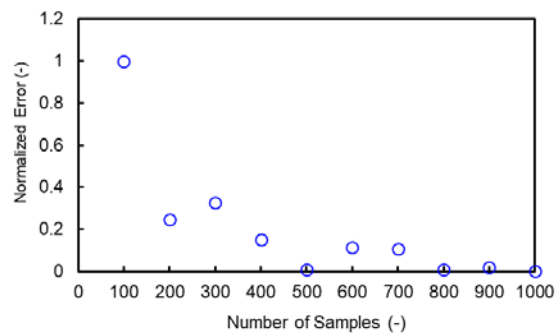


Figure 4-13: Brine leakage (kg/s) to groundwater aquifers over time (year). The numbers on top of each graph represent the amount of NRAP-IAM Monte Carlo simulations performed.

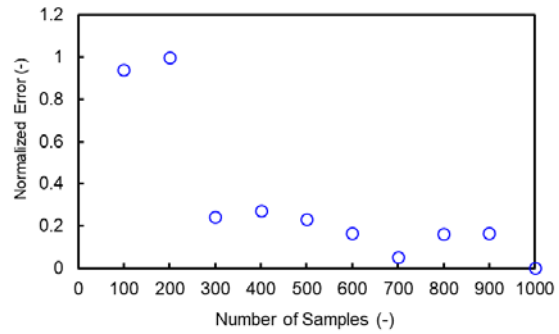
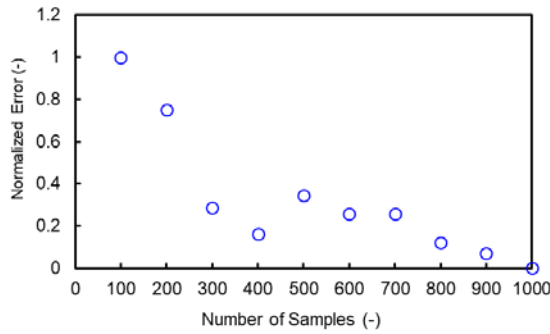
Using equation (11), error calculation was carried out to help determine the interval of convergence. **Figure 4-14** presents the error calculation results for CO_2 and brine leakage to an intermediate reservoir and groundwater aquifers versus number of samples/simulations performed. Some cases, especially the brine leakage cases are not fully converged even with the large number of realizations (**Figure 4-14**). This is because of the nature of Monte Carlo sampling in NRAP-IAM, meaning that NRAP-IAM shows slightly different results in every run. It is therefore reasonable to define the optimal number of realizations in NRAP-IAM runs as the number of realizations at which significant reduction of the error is seen. In this particular example, the convergence of NRAP-IAM may be the number of realizations of 400-500.



(a) CO_2 leakage to intermediate reservoir



(b) CO_2 leakage to groundwater aquifers



(c) Brine leakage to Intermediate Reservoir

(d) Brine leakage to groundwater aquifers

Figure 4-14: Error calculation results for NRAP-IAM

4.4. Discussion

The results of this risk assessment study consist of full-physics model sensitivity analysis, leakage through legacy wells, and leakage through fault pathways. These simulations are to address the initial questions regarding possibility of successfully injecting 1 mega ton (MT) of CO₂ into the Duperow formation as well as risk of leakage through wellbore and fault pathways.

Full-physics model injection simulations show that it is highly unlikely that the project will meet its target of 1 MT of CO₂ injection, given the current fracture permeability model. **Figure 4-4** depicts sensitivity of total CO₂ mass injection of 50 LHS E300 simulations after 4 years. Injection was under a BHP control of 18.5 MPa to avoid fracturing the formation. Based on this upper limit and the current fracture permeability model, total injection amounts rarely exceed 1 MT at the end of 4 years. In contrast to the results presented by Dai et al. (2014) which rely on data from a nearby well and indicate a reasonable likelihood of reaching total injectivity, our work employs measured data at the injection well and predicts a significantly lower chance of meeting the desired injection goal. Nonetheless, both studies present a single-well scenario and thus require more spatial information to address subsurface heterogeneity which has been proven to be among key factors that affect injectivity. Using core and detailed seismic data, an improved understanding of facies and fracture distributions can be incorporated into the next step of Kevin Dome reservoir injection simulations. The LHS sampling process in this study can be applied to similar uncertainty analysis studies with large numbers of sensitive parameters.

The study on leakage through legacy wells indicates very minimal CO₂/brine leakage to the atmosphere. However, there is still the possibility of CO₂ and brine migrating into an intermediate reservoir and contaminating groundwater aquifers. **Figures 4-9 to 4-13** indicate that leakage is more likely to occur during the 4 years of injection and tends to slow down afterwards as pressures dissipate. Overall, there is more CO₂ leakage to intermediate reservoirs and groundwater aquifers than brine, which is possibly related to buoyancy and mobility of supercritical CO₂. Leakage is most likely to happen at legacy well SUTA 2-26 (**Figure 3-10**) due to its vicinity to Wallewein 22-1 and because low fracture permeability does not allow the CO₂ plume to travel further away. However there is also the chance of converting a nearby well into an observation well as mentioned by Dai et al. (2014), which could potentially reduce the operational cost of a GCS project based

on predicting the CO₂ plume. In addition, these observations emphasize the importance of understanding the fracture network of Duperow formation and its associated fracture permeability.

On the other hand, NRAP-IAM risk assessment of leakage through faults presents a framework for evaluating flow across multiple formations through the use of ROMs instead of relying on simplified analytical models (Shan et al. 1995; Chang et al., 2008; Zeidouni, 2012). Simulation results reinforce the significance of reservoir heterogeneity regarding the leakage potential (**Figure 4-7**). Such studies on fault leakage apparently require a comprehensive understanding of the vertical and lateral extent of a fault as well as its flow-related properties. We found that the leakage amount is sensitive to fault displacement, although this parameter in the NRAP fault ROM is not well tied to validated values (**Figure 4-8**). This research provides a hypothetical case study that can be applied elsewhere to simulate fault leakage.

5. Summary and Future Work

In this study, we have conducted risk assessment of potential CGS into the middle Duperow formation at Kevin Dome, Montana using the hybrid NRAP-IAM model. Instead of running full-physics models, NRAP-IAM uses ROMs to perform a large number of simulations and explore many uncertain variables and their impact on CO₂ and brine leakage should actual CO₂ injection take place at the site. NRAP-IAM has proved itself to be a powerful tool to carry out such risk assessment studies given the ROMs and its compatibility with other reservoir simulators.

From the sensitivity analysis study of injection reservoir parameters, we found that the potential amount of CO₂ leakage is most sensitive to fracture permeability, end-point CO₂ relative permeability, capillary pressure, and permeability of confining rocks. Study on leakage pathways including legacy wells and faults was also carried out. We learned that wellbore integrity has the most impact on CO₂ leakage to the atmosphere within the first 10 years after injection. Monitoring the plume movement and identifying an accurate number of legacy wells are recommended. As for fault leakage pathways, fracture permeability has more impact on CO₂ leakage than brine leakage, allowing the supercritical and dissolved CO₂ to move laterally and reach the fault pipes. Fault displacement appears to exert a significant influence on both CO₂ and brine leakage in our study and should be well understood to ensure the safety of CGS operations.

Future study will incorporate more fault information/interpretation as well as facies and fracture-driven reservoir porosity and permeability models from Schlumberger to better address heterogeneity and predict plume dynamics during and post-injection. Modifications will be made to NRAP-IAM to improve its fault leakage model. Two manuscripts will be prepared to present current results and new ones with more heterogeneous reservoir models.

6. References

- Ahmadov, R., Aydin, A., Karimi-Fard, M., & Durlofsky, L. J. (2007). Permeability upscaling of fault zones in the Aztec Sandstone, Valley of Fire State Park, Nevada, with a focus on slip surfaces and slip bands. *Hydrogeology Journal*, 15(7), 1239-1250
- Annunziatellis, A., Beaubien, S. E., Bigi, S., Ciotoli, G., Coltella, M., & Lombardi, S. (2008). Gas migration along fault systems and through the vadose zone in the Latera caldera (central Italy): implications for CO₂ geological storage. *International Journal of Greenhouse Gas Control*, 2(3), 353-372.
- Bachu, S. (2000). Sequestration of CO₂ in geological media: criteria and approach for site selection in response to climate change. *Energy conversion and Management*, 41(9), 953-970.
- Bao, J., Hou, Z., Fang, Y., Ren, H., & Lin, G. (2013). Uncertainty quantification for evaluating impacts of caprock and reservoir properties on pressure buildup and ground surface displacement during geological CO₂ sequestration. *Greenhouse Gases: Science and Technology*, 3(5), 338-358.
- Barrufet, M. A., Bacquet, A., & Falcone, G. (2010). Analysis of the storage capacity for CO₂ sequestration of a depleted gas condensate reservoir and a saline aquifer. *Journal of Canadian Petroleum Technology*, 49(08), 23-31
- Bernabé, Y., Mok, U., & Evans, B. (2003). Permeability-porosity relationships in rocks subjected to various evolution processes. *Pure and Applied Geophysics*, 160(5), 937-960.
- Bidgoli, T. S., Watney, W. L., Gerlach, P. M., & Nguyen, M. C. (2014) Episodic reactivation of critically-stressed basement faults in southern Kansas: implications for wastewater disposal and long-term storage of CO₂. In 2014 GSA Annual Meeting in Vancouver, British Columbia.
- Blaskovich, F. T., Cain, G. M., Sonier, F., Waldren, D., & Webb, S. J. (1983). A multicomponent isothermal system for efficient reservoir simulation. In *Middle East Oil Technical Conference and Exhibition*. Society of Petroleum Engineers.
- Caine, J. S., Evans, J. P., & Forster, C. B. (1996). Fault zone architecture and permeability structure. *Geology*, 24(11), 1025-1028.
- Carey, J. W. (2017). *Probability Distributions for Effective Permeability of Potentially Leaking Wells at CO₂ Sequestration Sites*; NRAP-TRS-III-021-2017; NRAP Technical Report Series; U.S. Department of Energy, National Energy Technology Laboratory: Morgantown, WV; p 28.
- Carlson, F. M. (1981). Simulation of relative permeability hysteresis to the nonwetting phase. In *SPE Annual Technical Conference and Exhibition*. Society of Petroleum Engineers.
- Carroll, S., Carey, J. W., Dzombak, D., Huerta, N. J., Li, L., Richard, T., ... & Zhang, L. (2016a). Role of chemistry, mechanics, and transport on well integrity in CO₂ storage environments. *International Journal of Greenhouse Gas Control*, 49, 149-160.
- Carroll, S., Richard, T., and Bromhal, G., editors (2016b). Virtual Special Issue: National Risk Assessment Partnership. *International Journal of Greenhouse Gas Control*.
<https://www.journals.elsevier.com/international-journal-of-greenhouse-gas-control/virtual-special-issues/virtual-special-issue-national-risk-assessment-partnership>.

- Chang, K. W., Minkoff, S. E., & Bryant, S. L. (2008). Modeling leakage through faults of CO₂ stored in an aquifer. In SPE Annual Technical Conference and Exhibition. Society of Petroleum Engineers.
- Corey, A. T. (1954). The interrelation between gas and oil relative permeabilities. *Producers monthly*, 19(1), 38-41.
- Dai, Z., Stauffer, P. H., Carey, J. W., Middleton, R. S., Lu, Z., Jacobs, J. F., ... & Spangler, L. H. (2014). Pre-site characterization risk analysis for commercial-scale carbon sequestration. *Environmental science & technology*, 48(7), 3908-3915.
- Deng, H., Stauffer, P. H., Dai, Z., Jiao, Z., & Surdam, R. C. (2012). Simulation of industrial-scale CO₂ storage: multi-scale heterogeneity and its impacts on storage capacity, injectivity and leakage. *International Journal of Greenhouse Gas Control*, 10, 397-418.
- Eigestad, G. T., Dahle, H. K., Hellevang, B., Riis, F., Johansen, W. T., & Øian, E. (2009). Geological modeling and simulation of CO₂ injection in the Johansen formation. *Computational Geosciences*, 13(4), 435-450.
- Fairley, J., Heffner, J., & Hinds, J. (2003). Geostatistical evaluation of permeability in an active fault zone. *Geophysical Research Letters*, 30(18).
- Fakcharoenphol, P., Kurtoglu, B., Kazemi, H., Charoenwongsa, S., & Wu, Y. S. (2014, April). The effect of osmotic pressure on improve oil recovery from fractured shale formations. In SPE unconventional resources conference. Society of Petroleum Engineers.
- Fenghour, A., Wakeham, W. A., & Vesovic, V. (1998). The viscosity of carbon dioxide. *Journal of Physical and Chemical Reference Data*, 27(1), 31-44.
- Fourar, M., Bories, S., Lenormand, R., & Persoff, P. (1993). Two-phase flow in smooth and rough fractures: Measurement and correlation by porous-medium and pipe flow models. *Water Resources Research*, 29(11), 3699-3708.
- Harp, D. R., Pawar, R., Carey, J. W., & Gable, C. W. (2016). Reduced order models of transient CO₂ and brine leakage along abandoned wellbores from geologic carbon sequestration reservoirs. *International Journal of Greenhouse Gas Control*, 45, 150-162.
- Hill, M. C. (2000). Methods and guidelines for effective model calibration. In *Building Partnerships* (pp. 1-10).
- Hu, L., Pan, L., & Zhang, K. (2012). Modeling brine leakage to shallow aquifer through an open wellbore using T2WELL/ECO₂N. *International Journal of Greenhouse Gas Control*, 9, 393-401.
- Hyman, J. D., Karra, S., Makedonska, N., Gable, C. W., Painter, S. L., & Viswanathan, H. S. (2015). dfnWorks: A discrete fracture network framework for modeling subsurface flow and transport. *Computers & Geosciences*, 84, 10-19.
- Iman, R. L., & Conover, W. J. (1980). Small sample sensitivity analysis techniques for computer models. with an application to risk assessment. *Communications in statistics-theory and methods*, 9(17), 1749-1842.
- Jordan, A. B., Stauffer, P. H., Harp, D., Carey, J. W., & Pawar, R. J. (2015). A response surface model to predict CO₂ and brine leakage along cemented wellbores. *International Journal of Greenhouse Gas Control*, 33, 27-39.

- Juanes, R., Spiteri, E. J., Orr, F. M., & Blunt, M. J. (2006). Impact of relative permeability hysteresis on geological CO₂ storage. *Water Resources Research*, 42(12).
- Kazemi, H., Merrill Jr, L. S., Porterfield, K. L., & Zeman, P. R. (1976). Numerical simulation of water-oil flow in naturally fractured reservoirs. *Society of Petroleum Engineers Journal*, 16(06), 317-326.
- Keating, E. H., Fessenden, J., Kanjorski, N., Koning, D. J., & Pawar, R. (2010). The impact of CO₂ on shallow groundwater chemistry: observations at a natural analog site and implications for carbon sequestration. *Environmental Earth Sciences*, 60(3), 521-536.
- Keating, E. H., Harp, D. H., Dai, Z., & Pawar, R. J. (2016). Reduced order models for assessing CO₂ impacts in shallow unconfined aquifers. *International Journal of Greenhouse Gas Control*, 46, 187-196.
- Killough, J. E. (1976). Reservoir simulation with history-dependent saturation functions. *Society of Petroleum Engineers Journal*, 16(01), 37-48.
- Krevor, S., Blunt, M. J., Benson, S. M., Pentland, C. H., Reynolds, C., Al-Menhali, A., & Niu, B. (2015). Capillary trapping for geologic carbon dioxide storage—From pore scale physics to field scale implications. *International Journal of Greenhouse Gas Control*, 40, 221-237.
- Land, C. S. (1968). Calculation of imbibition relative permeability for two-and three-phase flow from rock properties. *Society of Petroleum Engineers Journal*, 8(02), 149-156.
- Lee, J. (1982). *Well testing*. New York: Society of Petroleum Engineers.
- Li, L., & Lee, S. H. (2006, January). Efficient field-scale simulation for black oil in a naturally fractured reservoir via discrete fracture networks and homogenized media. In *International Oil & Gas Conference and Exhibition in China*. Society of Petroleum Engineers.
- Lim, K. T., & Aziz, K. (1995). Matrix-fracture transfer shape factors for dual-porosity simulators. *Journal of Petroleum Science and Engineering*, 13(3-4), 169-178.
- Mathias, S. A., Hardisty, P. E., Trudell, M. R., & Zimmerman, R. W. (2009). Approximate solutions for pressure buildup during CO₂ injection in brine aquifers. *Transport in Porous Media*, 79(2), 265-284.
- McKay, M. D., Beckman, R. J., & Conover, W. J. (1979). Comparison of three methods for selecting values of input variables in the analysis of output from a computer code. *Technometrics*, 21(2), 239-245.
- Metz, B., Davidson, O., De Coninck, H., Loos, M., & Meyer, L. (2005). IPCC special report on carbon dioxide capture and storage. Intergovernmental Panel on Climate Change, Geneva (Switzerland). Working Group III.
- Mijic, A., LaForce, T. C., & Muggeridge, A. H. (2014). CO₂ injectivity in saline aquifers: The impact of non-Darcy flow, phase miscibility, and gas compressibility. *Water Resources Research*, 50(5), 4163-4185.
- Moinfar, A. (2013). Development of an efficient embedded discrete fracture model for 3D compositional reservoir simulation in fractured reservoirs, Doctoral Dissertation, University of Texas, Austin, TX (US)

- Monteagudo, J. E. P., & Firoozabadi, A. (2004). Control-volume method for numerical simulation of two-phase immiscible flow in two-and three-dimensional discrete-fractured media. *Water resources research*, 40(7).
- NETL (2015) Carbon Storage Alas, 5th Edition, National Energy Technology Laboratory
- Nguyen, M. C., Zhang, Y., Jun, L., Li, X., Bai, B., Haiqing, W., ... & Stauffer, P. H. (2017a). A geostatistical study in support of CO₂ storage in deep saline aquifers of the Shenhua CCS project, Ordos Basin, China. *Energy Proc.* doi, 10.
- Nguyen, M.C., & Stauffer, P.H. (2017). Understanding CO₂ Storage Into Deep Saline Aquifers at the Shenhua Site, Ordos Basin using Simulation-based Sensitivity Analysis (No. LA-UR-17-26981). Los Alamos National Laboratory (LANL).
- Nguyen, M.C., Zhang, X., Wei, N., Li, J., Li, X., Zhang, Y., and Stauffer, P.H. (2017b) An Object-based Modeling and Sensitivity Analysis Study in Support of CO₂ Storage in Deep Saline Aquifers at the Shenhua site, Ordos Basin, Geomechanics and Geophysics for Geo-Energy and Geo-Resources, <https://doi.org/10.1007/s40948-017-0063-5>
- Nguyen, M.C., Zhang, Y., Carey, J.W. & Stauffer, P.H. (2017c). Application of an Integrated Assessment Model to the Kevin Dome site, Montana (No. LA-UR-17-29925). Los Alamos National Laboratory (LANL).
- Noorishad, J., & Mehran, M. (1982). An upstream finite element method for solution of transient transport equation in fractured porous media. *Water Resources Research*, 18(3), 588-596.
- Nordbotten, J. M., Celia, M. A., Bachu, S., & Dahle, H. K. (2005). Semianalytical solution for CO₂ leakage through an abandoned well. *Environmental science & technology*, 39(2), 602-611.
- Nordbotten, J. M., Kavetski, D., Celia, M. A., & Bachu, S. (2008). Model for CO₂ leakage including multiple geological layers and multiple leaky wells. *Environmental science & technology*, 43(3), 743-749.
- Odling, N. E., Harris, S. D., & Knipe, R. J. (2004). Permeability scaling properties of fault damage zones in siliclastic rocks. *Journal of Structural Geology*, 26(9), 1727-1747.
- Olalotiti-Lawal, F., Onishi, T., Datta-Gupta, A., Fujita, Y., & Hagiwara, K. (2017). Post-Combustion CO₂ EOR Development in a Mature Oil Field: Model Calibration Using a Hierarchical Approach. In SPE Annual Technical Conference and Exhibition. Society of Petroleum Engineers.
- Onishi, T., Stauffer, P.H., Nguyen, M.C. and Carey, J.W. (2017) Big Sky Project Preliminary Results June 28, 2017, Los Alamos National Laboratory, LA-UR-17-25222
- Pawar, R. J., Bromhal, G. S., Chu, S., Dilmore, R. M., Oldenburg, C. M., Stauffer, P. H., ... & Guthrie, G. D. (2016). The National Risk Assessment Partnership's integrated assessment model for carbon storage: A tool to support decision making amidst uncertainty. *International Journal of Greenhouse Gas Control*, 52, 175-189.
- Pawar, R., Carey, J., Chipera, S., Fessenden, J., Kaszuba, J., Keating, G., ... & Ziock, H. (2006). Development of a framework for long-term performance assessment of geologic CO₂ sequestration sites. In Eighth International Conference on Greenhouse Gas Control Technologies (GHGT-8) (pp. 19-22).

- Pieters, D. A., & Graves, R. M. (1994). Fracture relative permeability: linear or non-linear function of saturation. In International Petroleum Conference and Exhibition of Mexico. Society of Petroleum Engineers.
- Pruess, K., & Garcia, J. (2002). Multiphase flow dynamics during CO₂ disposal into saline aquifers. *Environmental Geology*, 42(2), 282-295.
- Pruess, K., & Spycher, N. (2009). Enhanced geothermal systems (EGS) with CO₂ as heat transmission fluid--A scheme for combining recovery of renewable energy with geologic storage of CO₂ (No. LBNL-1949E). Ernest Orlando Lawrence Berkeley National Laboratory, Berkeley, CA (US).
- Pruess, K., Oldenburg, C. M., & Moridis, G. J. (1999). TOUGH2 user's guide version 2 (No. LBNL--43134). Ernest Orlando Lawrence Berkeley National Laboratory, Berkeley, CA (US).
- Redlich, O., & Kwong, J. N. (1949). On the Thermodynamics of Solutions. V. An Equation of State. Fugacities of Gaseous Solutions. *Chemical reviews*, 44(1), 233-244.
- Rinaldi, A. P., Vilarrasa, V., Rutqvist, J., & Cappa, F. (2015). Fault reactivation during CO₂ sequestration: Effects of well orientation on seismicity and leakage. *Greenhouse Gases: Science and Technology*, 5(5), 645-656.
- Ringrose, P. S., Mathieson, A. S., Wright, I. W., Selama, F., Hansen, O., Bissell, R., ... & Midgley, J. (2013). The In Salah CO₂ storage project: lessons learned and knowledge transfer. *Energy Procedia*, 37, 6226-6236.
- Romm, E. S. (1966). Flow characteristics of fractured rocks. Nedra, Moscow, 283.
- Schlumberger (2015) ECLIPSE Technical Description Version 2015.2
- Shan, C., Javandel, I., & Witherspoon, P. A. (1995). Characterization of leaky faults: Study of water flow in aquifer-fault-aquifer systems. *Water Resources Research*, 31(12), 2897-2904.
- Shipton, Z. K., Evans, J. P., Robeson, K. R., Forster, C. B., & Snelgrove, S. (2002). Structural heterogeneity and permeability in faulted eolian sandstone: Implications for subsurface modeling of faults. *AAPG bulletin*, 86(5), 863-883.
- Shipton, Z. K., Evans, J. P., Dockrill, B., Heath, J., Williams, A., Kirchner, D., & Kolesar, P. T. (2006). Natural leaking CO₂-charged systems as analogs for failed geologic storage reservoirs. Carbon dioxide capture for storage in deep geologic formations—results from the CO₂ capture project, 2, 699-712.
- Singh, V. P., Cavanagh, A., Hansen, H., Nazarian, B., Iding, M., & Ringrose, P. S. (2010). Reservoir modeling of CO₂ plume behavior calibrated against monitoring data from Sleipner, Norway. In SPE annual technical conference and exhibition. Society of Petroleum Engineers.
- Soltanian, M. R., Amooie, M. A., Cole, D. R., Graham, D. E., Hosseini, S. A., Hovorka, S., ... & Moortgat, J. (2016). Simulating the Cranfield geological carbon sequestration project with high-resolution static models and an accurate equation of state. *International Journal of Greenhouse Gas Control*, 54, 282-296.
- Sorkhabi, R., & Tsuji, Y. (2005). The place of faults in petroleum traps. In *Faults, fluid flow, and petroleum traps*, Sorkhabi, R and Y Tsuji, Eds. AAPG Memoir Vol. 85, pp 1-31.

- Spangler, L. (2016) Big Sky Regional Carbon Sequestration Partnership – Kevin Dome Carbon Storage, National Energy Technology Laboratory
- Spycher, N., & Pruess, K. (2005). CO₂-H₂O mixtures in the geological sequestration of CO₂. II. Partitioning in chloride brines at 12–100 C and up to 600 bar. *Geochimica et Cosmochimica Acta*, 69(13), 3309-3320.
- Stauffer, P. H., Dai, Z., Lu, Z., Middleton, R. S., Jacobs, J. F., & Carey, J. W. (2013). LANL Deliverable to the Big Sky Carbon Sequestration Partnership: Preliminary CO₂-PENS model (No. LA-UR-13-22466). Los Alamos National Laboratory (LANL).
- Stauffer, P. H., Viswanathan, H. S., Pawar, R. J., Klasky, M. L., & Guthrie, G. D. (2006). CO₂-PENS: A CO₂ sequestration systems model supporting risk-based decisions. In *Proceedings of the 16th International Conference on Computational Methods in Water Resources* (pp. 19-22).
- Stauffer, P.H., Chu, S., Tauxe, C. and Pawar, R. (2015) NRAP Integrated Assessment Model-Carbon Storage (NRAP-IAM-CS) Tool User's Manual, NRAP-TRS-III-00X-2015, LA-UR-15-26073.
- Tauxe, C. and Stauffer, P.H. (2015) NRAP-IAM-CS Viewer User Manual, LA-UR-15-26203.
- Trautz, R. C., Pugh, J. D., Varadharajan, C., Zheng, L., Bianchi, M., Nico, P. S., ... & Dafflon, B. (2012). Effect of dissolved CO₂ on a shallow groundwater system: A controlled release field experiment. *Environmental science & technology*, 47(1), 298-305.
- Vasco, D. W., & Datta-Gupta, A. (2016). *Subsurface Fluid Flow and Imaging: With Applications for Hydrology, Reservoir Engineering, and Geophysics*. Cambridge University Press.
- Vesovic, V., Wakeham, W. A., Olchowky, G. A., Sengers, J. V., Watson, J. T. R., & Millat, J. (1990). The transport properties of carbon dioxide. *Journal of physical and chemical reference data*, 19(3), 763-808.
- Viswanathan, H. S., Pawar, R. J., Stauffer, P. H., Kaszuba, J. P., Carey, J. W., Olsen, S. C., ... & Guthrie, G. D. (2008). Development of a hybrid process and system model for the assessment of wellbore leakage at a geologic CO₂ sequestration site. *Environmental science & technology*, 42(19), 7280-7286.
- Warren, J. E., & Root, P. J. (1963). The behavior of naturally fractured reservoirs. *Society of Petroleum Engineers Journal*, 3(03), 245-255.
- White, M. D., Bacon, D. H., McGrail, B. P., Watson, D. J., White, S. K., & Zhang, Z. F. (2012). STOMP subsurface transport over multiple phases: STOMP-CO₂ and STOMP-CO₂e guide: version 1.0 (No. PNNL-21268). Pacific Northwest National Laboratory (PNNL), Richland, WA (US).
- Wilkin, R. T., & DiGiulio, D. C. (2010). Geochemical impacts to groundwater from geologic carbon sequestration: controls on pH and inorganic carbon concentrations from reaction path and kinetic modeling. *Environmental Science & Technology*, 44(12), 4821-4827.
- Yoshida, N., Levine, J. S., & Stauffer, P. H. (2016). Investigation of uncertainty in CO₂ reservoir models: A sensitivity analysis of relative permeability parameter values. *International Journal of Greenhouse Gas Control*, 49, 161-178.

- Zaluski, W. (2017) MSU Slide Geomodel 3 Review Call May 2, 2017, Schlumberger
- Zeidouni, M. (2012). Analytical model of leakage through fault to overlying formations. *Water Resources Research*, 48(12).
- Zhou, Q., Oldenburg, C. M., Spycher, N., Pan, L., & Cihan, A. (2013). Milestone Report: Summary of Site Characterization, Data Collection and Review, Development of Static Geologic Model, and Preliminary Multiphase Flow and Reactive Transport Modeling Activities. United States. doi:10.2172/1164512
- Zhou, Q., Oldenburg, C. M., Spangler, L. H., & Birkholzer, J. T. (2017a). Approximate solutions for diffusive fracture-matrix transfer: Application to storage of dissolved CO₂ in fractured rocks. *Water Resources Research*, 53(2), 1746-1762.
- Zhou, Q., Oldenburg, C. M., Rutqvist, J., & Birkholzer, J. T. (2017b). Revisiting the Fundamental Analytical Solutions of Heat and Mass Transfer: The Kernel of Multirate and Multidimensional Diffusion. *Water Resources Research*.
- Zoback, M. D., & Gorelick, S. M. (2012). Earthquake triggering and large-scale geologic storage of carbon dioxide. *Proceedings of the National Academy of Sciences*, 109(26), 10164-10168.
- Zyvoloski, G. (2007). FEHM: A control volume finite element code for simulating subsurface multi-phase multi-fluid heat and mass transfer. Los Alamos Unclassified Report LA-UR-07-3359.